This is a preprint, the final version is subject to change, of the American Mineralogist (MSA)
Cite as Authors (Year) Title. American Mineralogist, in press.
DOI: https://doi.org/10.2138/am-2018-6520

Revision 1

The role of crustal melting in the formation of rhyolites: constraints from SIMS oxygen isotope data (Chon Aike Province, Patagonia, Argentina)

Susanne Seitz[1*], Benita Putlitz[1*], Lukas Peter Baumgartner[1], Anne-Sophie Bouvier[1]

[1]Institute for Earth Sciences, University of Lausanne, CH-1015 Lausanne, Switzerland

[*]*corresponding author:* susanne.seitz@unil.ch; benita.putlitz@unil.ch

Abstract

We report on the oxygen isotope composition of Jurassic rhyolites from a silicic large igneous province, the Chon Aike Province (Patagonia, Argentina). Quartz is shown to behave refractory with respect to diffusional oxygen isotope exchange, making it a robust tracer of magmatic processes. Detailed SIMS (secondary ion mass spectroscopy) transects across 24 quartz crystals reveal homogeneous, but elevated, oxygen isotope values (10.9 - 12.5 ‰). None of the analyzed grains display distinct discontinuities in ^{18}O values. Late hydrothermal exchange is limited to a few tens of micrometer next to cracks, some grain boundaries, and inclusions. No correlation with igneous zoning as revealed by cathodoluminescence (CL) was found. Finally, quartz crystals display little to no inter-grain variability at sample or outcrop scale. Zircons (7.5 – 10.1 ‰), in contrast, display significant inter-crystalline oxygen isotopic heterogeneity (> 2.0 ‰) at sample scale, but core-rim analyses reveal no systematic variations. This is interpreted to confirm the antecrystic nature of zircons, while quartz crystals mostly are phenocrysts. The

Always consult and cite the final, published document. See http:/www.minsocam.org or GeoscienceWorld

studied quartz and zircon provide, hence, complementary information on the evolution of magmatic system of the Chon Aike Province. Zircon likely captures information about the deeper source region, in contrast to quartz that will record the last stages of the magmatic system and thus might provide important information on the build-up and duration of magma chamber processes in the upper crust. The data illustrate that quartz - in absence of recrystallization - can retain its magmatic signature and is thus a useful tracer of pre-eruptive magmatic processes. The high $\delta^{18}O$ values of both zircon and quartz require significant (> 50 %) crustal - most likely sedimentary – contribution in the melt formation process, either via assimilation or anatexis. This yields new constraints on petrological models for the Chon Aike Province.

Introduction

Deciphering magmatic process using oxygen isotopes has made important progress over the last decade due to in-situ SIMS analysis mainly on the minerals zircon and olivine (Valley 2003; Bindeman 2008; Wang and Eiler 2008; Eiler et al. 2011; Bowman et al. 2012; Manzini et al. 2017). In silica-rich chemistries, e.g., granites and rhyolites, zircon is the mineral of choice for oxygen isotope analyses since it is a robust tracer of magmatic processes, and it can be combined with in-situ U-Pb age dating and trace element analysis (Wotzlaw et al. 2014). Compared to zircon, systematic in-situ oxygen isotope analysis of intra- and inter-grain variation of quartz is still rare, despite its abundance as phenocryst and the great interest in quartz textures, quartz thermometry and diffusion chronometry (Wark and Spear 2005; Wark and Watson 2006; Cherniak et al. 2007; Wark et al. 2007; Saunders et al. 2010; Thomas et al. 2010; Gualda et al. 2012; Huang and Audétat 2012; Matthews et al. 2012b; Chamberlain et al. 2014; Seitz et al. 2016b, Seitz et al. 2018), and especially considering that the diffusion parameters for oxygen

Always consult and cite the final, published document. See http:/www.minsocam.org or GeoscienceWorld

47 isotope in quartz are among the best known (Dennis 1984; Giletti and Yund 1984; Sharp et al.
48 1991).
49
50 Since quartz is a major rock forming component in acidic rocks, it was always part of the
51 analytical suite in oxygen isotopes works and is still routinely analyzed (e.g. Grunder and
52 Wickham 1991; Masuda and O'Neil 1994; King and Valley 2001; Bindeman and Valley 2001;
53 Bindeman 2008; Fourie and Harris 2011; Watts et al. 2011; Folkes at al. 2013; Watts et al. 2016;
54 Ellis et al. 2017 among many others). Nevertheless, its importance as tracer of magmatic
55 processes appears diminished, because it has been questioned to which extent quartz - as
56 opposed to zircon - retains it magmatic signature. The works of Valley and Graham 1996 and
57 King et al. 1997 clearly demonstrated that quartz can be affected by post-magmatic hydrothermal
58 fluid-rock interaction (see also Allan and Yardley 2007; Tanner et al. 2013; Fekete et al. 2016).
59 Additional arguments come from quartz-zircon oxygen isotope systematics: zircon and quartz
60 are rarely in high-temperature equilibrium, even in fast cooling extrusive rocks (e.g., Bindeman
61 and Valley 2002). This observation of disequilibrium persists, despite the uncertainties in the
62 fractionation factors applied, and has been used to support the general view that quartz is more
63 susceptible to secondary exchange processes. Yet, as pointed out by Valley and Graham 1996,
64 the isotopic gradients that must exist in partially exchanged quartz grains have not been well
65 documented. The high lateral spatial resolution of about 10 to 15 μm of the secondary ion mass
66 spectrometry analysis is ideal to have a closer look at the oxygen isotope systematics of quartz
67 and its zoning. Oxygen isotope zonation in quartz is also interesting, in view of the abundant
68 cathodoluminescence zonation observed in quartz and the recent use of Ti-diffusion chronometry

Always consult and cite the final, published document. See http:/www.minsocam.org or GeoscienceWorld

(Wark et al. 2007; Saunders et al. 2010; Gualda et al. 2012; Matthews et al. 2012a; 2012b; Chamberlain et al. 2014; Seitz et al. 2016b; Seitz et al. 2018).

Only a few studies to date, however, have analyzed the oxygen isotope composition of magmatic quartz using in-situ techniques in a systematic manner (Valley and Graham 1996; Allan and Yardley 2007; Tanner et al. 2013, Fekete et al. 2016; Ankney et al. 2017; Budd et al. 2017). Here we report on the oxygen isotope signature of quartz and zircon from a suite of silicic volcanic rocks of Jurassic age that forms part of the Chon Aike magmatic province in Patagonia (Argentina). In particular, we are interested to evaluate if quartz can retain its magmatic isotope signature, and to explore how quartz compared to zircon can provide complementary information on the magmatic evolution. Thus, a goal of our study was (a) to examine whether individual quartz phenocrysts are homogeneous or zoned in $\delta^{18}O$, (b) to assess the grain-to-grain variability in each sample, and (c) to determine how variations in $\delta^{18}O$ can be correlated with textural features (on grain- or hand sample scale), and (d) how their values compare to zircon $\delta^{18}O$. We discuss the likely mechanisms, such as recrystallization, diffusion or fluid infiltration via cracks, that produce the variability – or absence thereof – in $\delta^{18}O$.

We further use the quartz data in combination with in-situ zircon analysis to discuss potential magma sources. Oxygen isotope data on rhyolites are scarce in Patagonia (Riley et al. 2001), and our data provide novel constraints on the role of crustal melting in the formation of the Chon Aike magmatic province.

Geological setting

Always consult and cite the final, published document. See http:/www.minsocam.org or GeoscienceWorld

The investigated suite of Jurassic rhyolitic lava flows and ignimbrites belong to the Chon Aike magmatic Province (CAP). This province is considered to be one of the world's largest silicic provinces (SLIP; Bryan et al. 2002; Bryan and Ferrari 2013), with an estimated volume of about 235000 km^3 (Pankhurst et al. 1998). Because of its importance for the understanding of the Jurassic tectonic setting and ore-forming processes, this province has attracted considerable attention. For details on the CAP see papers by Baker et al. 1981; Gust et al. 1985; Kay et al. 1989; Wever and Storey 1992; Pankhurst and Rapela 1995; Pankhurst et al. 1998; Riley and Leat 1999; Pankhurst et al. 2000; Riley and Knight 2001; Riley et al. 2001; 2010; Japas et al. 2013; Benedini et al. 2014; Sruoga et al. 2014, as well as Pankhurst et al. 2011 and recent papers by Navarrete et al. 2016; Angiboust et al. 2017; Bouhier et al. 2017; Dopico et al. 2017. Yet, despite the important work accomplished, the CAP is not as well investigated as the large silicic systems in the western US or New Zealand for example.

The CAP developed in an extensional setting during the initial stage of the continental breakup of Gondwana. The products of this Jurassic volcanism cover a large area in Patagonia, from the Tierra del Fuego in the south to the North Patagonian Massif (Fig. 1). Volcanism was active for about 40 My and partly coincides with the Karroo-Ferrar mafic magmatism (e.g., Pankhurst et al. 2000; Riley et al. 2004). Pankhurst et al. 2000 distinguished three main volcanic episodes: the oldest episode (V1) occurred between 188 and 178 Ma, the second episode (V2) between 172 and 162 Ma and the youngest episode (V3) between 157 and 153 Ma. The age progression of the province is consistent with the migration of magmatism away from a mantle plume towards a proto-pacific margin (Riley and Leat 1999; Pankhurst et al. 2000; Riley et al. 2001). It is associated with NE-SW direction of extensional opening (Mpodozis and Ramos 2008).

Always consult and cite the final, published document. See http:/www.minsocam.org or GeoscienceWorld

Contemporaneously, subduction along the proto-pacific margin of Gondwana moved southwards along the western margin of South America during the Jurassic (Mpodozis and Ramos 2008). This change is also documented in the geochemical characteristic of the different volcanic episodes. The V1 episode (in northeast Patagonia and in the south of the Antarctic Peninsula) shows intraplate characteristics in response to mafic underplating associated with the Karoo-Ferrar mantle plume. Magmatism shifted to southern Patagonia and the northern Antarctic Peninsula during the V2 episode. The geochemistry of those rocks shows a signature of anatexis of a less evolved hydrous mafic crust, which is thought to be linked to pre-Middle Jurassic arc-related underplating. The V3 igneous rocks in the southern Andes are the result of a significant westwards shift in volcanic activity. They show an active-margin signature and are associated with granitoids (Pankhurst et al. 2000) and they are coeval with the emplacement of the oldest parts of the South Patagonian Batholith (145 and 157 Ma; Hervé et al. 2007b).

The importance of crustal melting in the formation of the silicic CAP has been pointed out by several influential papers. Early geochemical studies (Baker et al. 1981; Gust et al. 1985; Wever and Storey 1992) argued that significant crustal melting was necessary to obtain the rhyolitic volcanic rocks of the CAP. Later, Pankhurst and Rapela (1995 and follow-up papers) suggested that the formation of the CAP rhyolites was due to partial melting of a mafic, granulite-facies lower crust of Grenvillain (model) age. The produced initial andesitic parental magma further evolved by fractional crystallization, likely in multiple stages (Pankhurst et al. 1998). Pankhurst and Rapela (1995) ruled out a significant contribution from a heterogeneous upper crust (see also Riley et al. 2001), also because the $^{87}Sr/^{86}Sr$ ratios of rhyolitic rocks are relatively homogenous throughout the CAP with values close to 0.7068.

Always consult and cite the final, published document. See http:/www.minsocam.org or GeoscienceWorld

137

138 **Study area and sample description**

139 The study area (Fig. 1 and Fig. 2) is located in southern Patagonia in the Fitz Roy mountain
140 range (Argentina), east of the Chaltén Plutonic Complex (Ramírez de Arellano et al. 2012). In
141 this part of Patagonia, the Jurassic volcanic rocks of the CAP are known as El Quemado
142 Complex (EQC). In the study area, the EQC is composed of several rhyolitic flows and domes
143 (further referred to as flows) and associated rhyolitic volcanoclastic rocks (further referred to as
144 ignimbrites). The flows form kilometer-sized bodies, and are intercalated with the Rio Mayer
145 Formation, a Cretaceous pelitic sequence (Fig. 3a). They preserved magmatic flow banding and
146 vesicles (Fig. 3b). The sample localities Cerro Madsen, Laguna Sucia, Half Moon and the Loma
147 de las Pizarras are shown in Fig. 2. Ignimbrites are exposed at the Cerro Polo locality (Fig. 2).
148 Here a series of slightly inclined ignimbrite strata contain variable amounts of volcanic bombs
149 and lithic fragments, and they are often characterized by fiamme structures (Fig. 4b and c). The
150 ignimbrites discordantly overly a Paleozoic Basement, the Bahía de la Lancha Formation (Fig.
151 4a).

152

153 U-Pb zircon data from flows (Half Moon, Loma des Piazarras) and ignimbrites (Cerro Polo)
154 yield Jurassic ages between 153 - 148 Ma (Leresche 2013); they belong thus to youngest (V3)
155 episode of Jurassic volcanic activity in agreement with data from Malkowski et al. 2015 and
156 studies further away (Pankhurst et al. 2000; Fildani and Hessler 2005). Representative whole
157 rock analysis of the EQC are given in Table 1 and plotted in Fig. 5. The investigated flows and
158 ignimbrites are peralumineous and show high SiO_2 contents from 75 to 82 wt% and Al_2O_3 varies
159 between 12 and 15 wt%. Rocks of the EQC are typically low in MgO (< 1 wt%) and TiO_2 (< 0.5

Always consult and cite the final, published document. See http:/www.minsocam.org or GeoscienceWorld

wt%). In this characteristic they compare well with previously published data (e.g., Pankhurst and Rapela 1995) from silicic volcanics throughout the CAP (see Fig.5). Alteration lead to replacement of matrix and feldspar by carbonate and clay minerals. It is evident in low K_2O and elevated CaO-contents (see circled field in Fig.5).

Observation from thin sections and X-ray tomography show that the investigated flows are crystal-poor, while ignimbrites are crystal-rich (see also Seitz et al. 2018). Flows contain between 4 and 6 % quartz and sometimes up to 4 % feldspar crystals in a very fine-grained matrix of quartz and feldspar, which is interpreted to be recrystallized glass. Accessory biotite, zircon, and secondary ilmenite is present. Quartz crystals are mostly subhedral, with some embayments. Quartz shows magmatic oscillatory zoning in cathodoluminescence (CL) images (Fig. 6). Some of the quartz crystals contain inclusions or embayments of recrystallized melt. Ignimbrites are crystal rich and contain between 15 and 25 % quartz and between 10 and 15 % feldspar crystals in a very fine-grained matrix of quartz and feldspar. Accessories are biotite, zircon and secondary ilmenite. The matrix and the feldspars are frequently replaced by carbonate minerals. In CL images quartz crystals show a large variety in magmatic zoning patterns (Fig 7) with oscillatory, normal and reverse zoning along with internal dissolution textures. A detailed description and discussion of the quartz zoning pattern and can be found in Seitz et al., 2018.

Analytical Methods

Oxygen isotope analysis by CO_2–laser fluorination

Oxygen isotope data were acquired in the stable isotope laboratory of the University of Lausanne (Switzerland). Whole rock powder aliquots of 1 - 2 mg and handpicked quartz grains (1-3

Always consult and cite the final, published document. See http:/www.minsocam.org or GeoscienceWorld

individual crystals) were analyzed using the CO_2-laser fluorination method (for details on the procedure in Lausanne see Lacroix and Vennemann 2015). Results are corrected either to the international quartz standard NBS-28 (9.64 ‰, Coplen et al. 1983) or to the in-house standard LS-1 quartz, which has been calibrated to be 18.1 ‰ against NBS-28. The average precision and accuracy on replicates of these standards is better than 0.1 ‰.

SIMS $\delta^{18}O$ measurements of quartz and zircon

The oxygen isotope composition of quartz and zircon was measured in the SwissSIMS laboratory at the University of Lausanne (Switzerland). Central cuts of quartz phenocrysts were prepared for SIMS analysis based on 3D-images using computed micro X-ray tomography (μCT). Rock cores (~1.5 cm diameter and ~3 cm length) were marked with small saw cuts (using a wire saw) and subsequently imaged using a Bruker-SkyScan1173® μCT instrument. Scan-time was 14-15 hours, at 70 kV/140 nA or 80 kV/100 nA with a step size of 0.23° for a 360° rotation and averaging of 40 frames per rotation step. Volume rendering and image analysis were achieved using the SkyScan® software package. Quartz crystals were chosen based on their sizes and shape. Once the center of a crystal was identified, a ~1 mm thick section was prepared (i.e. the rock cores were cut slightly above or below the center identified of the chosen quartz crystal) and then carefully polished down to obtain sections that yield quartz cross sections corresponding to the central cut as identified in the tomographic images (see also Skora et al. 2006). Zircons were extracted from the hand sample using the electrodynamic disaggregation method (for details see Giese et al. 2010) at the SelFrag laboratory of the Institute of Geology, University of Bern (Switzerland). The samples were sieved and the zircons were concentrated from the <125 μm fraction based on density. Zircons were handpicked from this concentrate.

Always consult and cite the final, published document. See http:/www.minsocam.org or GeoscienceWorld

206

207 The extracted quartz and zircon crystals were mounted together with the UNIL-Q1 quartz
208 standard (Seitz et al. 2016a) and the Penglai zircon (Li et al. 2010) respectively. Care was taken
209 to only use the innermost 15 mm of the 2.5 cm diameter epoxy mount. The epoxy mount was
210 polished with diamond paste, successively reducing grain size from 15 to 0.5 μm.
211 Cathodoluminescence (CL) images were collected for each mount using the CamScanMV2300
212 scanning electron microscope (University of Lausanne).

213

214 The $^{18}O/^{16}O$ ratios were measured using a Cameca IMS 1280HR instrument. We used a 10 kV
215 Cs^+ primary beam, a ~2 nA current, resulting in a ~10 μm beam size. The electron flood gun,
216 with normal incidence, was used to compensate charges. ^{16}O and ^{18}O secondary ions, accelerated
217 at 10 kV, were analyzed at a mass resolution of 3000 and collected on faraday cups in multi-
218 collection mode. Faraday cups are calibrated in the beginning of the session, using the calibration
219 routine. Each analysis takes less than 4 minutes, including pre-sputtering (30 sec) and automated
220 centering of secondary electrons. A set of four standard analyses was measured every 10 - 20
221 analyses to monitor the instrument stability.

222

223 **Results**

224 **Oxygen isotope geochemistry of quartz**

225 We conducted a detailed SIMS study with over 600 quartz analyses covering 5 samples from
226 flows and 6 samples from ignimbrites. This dataset is complemented by laser-fluorination
227 analyses. Detailed ion microprobe $\delta^{18}O$ traverses were measured across 24 grains, 11 grains from
228 flows and 13 grains from ignimbrites. CL imaging was used to select the best profile directions,

Always consult and cite the final, published document. See http:/www.minsocam.org or GeoscienceWorld

so as to travers as many zones possible. Profiles are between 200 µm to 1500 µm long. If judged interesting, multiple profiles were obtained on a single grain, resulting in a total of 34 profiles, of which 17 are from flows and 17 are from ignimbrites. The data are summarized in Table 2a and 2b. All data is given in Supplement Table 1. Grains labeled #1-11 are from flows, while grains #12-24 are from ignimbrites.

Intra-grain variations. The SIMS $\delta^{18}O$ profiles on quartz grains are quite homogenous no systematic zoning is apparent, considering the reproducibility of ca. 0.3 ‰ (see Fig. 6 to Fig. 8). None of the analyzed grains display distinct discontinuities in ^{18}O values that corresponds spatially with a core-rim boundary or zonation as defined in CL, which in these grains is tightly correlated with the Ti-variations, interpreted to reflect growth structures (Seitz et al. 2016b, Seitz et al. 2018).

The intra-grain homogeneity is well illustrated in the ignimbrite samples (grains #12 to #24) where $\delta^{18}O$–profiles traverse several CL zones but are flat and yield $\delta^{18}O$ values between 10.8 ‰ and 11.1 ‰ (Fig. 7 and Fig. 8). A particularly nice example is grain #24 (in sample ign-A10) which has a bright CL rim, but no corresponding $\delta^{18}O$ signal, or grain #20 (sample ign-A5) with its complex CL zoning. Potential non-concentric oxygen isotope zoning was investigated with two or more profiles (see e.g. grain #12 in sample ign-B3). Individual traverses were either obtained at a high angle to each other or parallel to each other. No zoning was found, confirming that quartz phenocrysts are homogenous taking into account ca. 0.3 ‰ (2 sigma) of the SIMS analysis.

Always consult and cite the final, published document. See http:/www.minsocam.org or GeoscienceWorld

Profiles of $\delta^{18}O$ across quartz from flows (grains #1 to #11) are typically more variable (Fig. 6 and Fig 8). Discrete shifts in $\delta^{18}O$ values are observed near grain boundaries, along healed cracks (dark in CL, but no surface topography) and embayments or melt inclusions. Most common are shifts to slightly higher values (from 11.5 - 12.0 ‰ to 13.0 - 14.0 ‰). Nevertheless, some lower values were also measured. In general, grains from the flows show more healed cracks than grains in ignimbrites, with a few exceptions (see e.g. grain #12 from sample ignSLB3). Cracks usually crosscut CL-domains. Note, that not all cracks result in a $\delta^{18}O$ shift. Indeed, there are many examples were cracks do not disturb the ^{18}O pattern. The width of healed cracks as seen in 2D also does not correlate with the extent of ^{18}O changes: sometimes small cracks induce a pronounced shift, larger than a big crack. A shift towards higher $\delta^{18}O$ values near an embayment or a recrystallized melt inclusion can be observed in grain #3 and to a smaller extend in grain #9. However, the shift in ^{18}O values does not correlate to the distinct zonation seen in the CL images.

Crystal to Crystal variation on a hand sample and outcrop scale. We have analyzed between 2 and 5 grains in seven of the samples (3 ignimbrites and 4 flows) to test for grain-to-grain variability (see Fig. 6 to Fig. 8 and Fig. S1 in the data repository). Most samples exhibit no inter-grain variability exceeding the 0.3 ‰ level of the reproducibility of the SIMS analysis. The exception is flow sample rhyPN73 from the Loma de las Pizarras; one grain has a slightly higher average composition when compared to the three other grains from this sample (Tab. 2b) but is still within error of the other grains.

Always consult and cite the final, published document. See http:/www.minsocam.org or GeoscienceWorld

The comparison of samples – using both SIMS and laser fluorination data (see below) - from any specific outcrop or location shows that they yield very similar quartz compositions. All ignimbrites were collected in the Cerro Polo area. To assess the extent of lateral and vertical variations we analyzed quartz crystals from several samples within a stratigraphic unit of the Cerro Polo section. Samples from the same tuff unit (e.g., grains #20 and #21 from layer 9 of the Cerro Polo section, or grains #22 to #24 from layer 8 of the section) are indistinguishable within error, and the Cerro Polo section as a whole is homogenous ($\delta^{18}O$ of 10.8 to 11.2 ‰). Flows sampled at the Half Moon and Loma de las Pizarras, are characterized by $\delta^{18}O$ values between 11.4 ‰ and 12.3 ‰. The flows from Cerro Madsen can be distinguished from the latter two localities, they show slightly higher $\delta^{18}O$ values of 12.6 – 13.4 ‰.

Laser fluorination $\delta^{18}O$ data of whole rock and quartz

The SIMS work was complemented by laser fluorination analysis (Tab. 2a). We investigated whole rocks (23 flows, 7 ignimbrites) and quartz crystals (9 flows and 2 ignimbrites). The whole rock $\delta^{18}O$ data for flows and ignimbrites differ significantly. Most of the whole rock data from flows cover a range between ca. 11 – 13 ‰ (see Tab. 2a). These values are similar to the $\delta^{18}O$ quartz values, which works well with the fact, that fractionation between a rhyolitic magma and quartz is small at high temperature (0.8 ‰ at 700°C and 0.5 ‰ at 900°C, see discussion below). In contrast, ignimbrite samples show significantly elevated $\delta^{18}O$ whole rock values of ca. 15 – 16 ‰ (Tab. 2a), while quartz values vary between 11.0 – 11.4 ‰. Thin section observation and XRF analyses confirm that high $\delta^{18}O$ signature of the ignimbrites are clearly the result of secondary alteration. Much of the matrix and the feldspar crystals are replaced by carbonate minerals. Hydrothermal alteration is also confirmed by the whole rock chemical data plotted in

Always consult and cite the final, published document. See http:/www.minsocam.org or GeoscienceWorld

297 Fig 5. They have low alkali concentrations, which is compensated by elevated a CaO content.
298 Interestingly, although the whole rock oxygen isotope signatures of these ignimbrite are the
299 result of alteration, this does not appear to affect the oxygen isotope value of the quartz (see
300 discussion below).
301
302 **Comparison of laser fluorination and SIMS data**
303 SIMS analysis has demonstrated that quartz grains from ignimbrites are homogeneous. The
304 average value obtained from SIMS analysis compares well with those obtained from laser
305 fluorination analyses. The same applies to samples from flows; an exception is sample rhyL5
306 from the Cerro Madsen locality (Tab. 2a), where the laser fluorination value is slightly lower
307 (12.5 ‰) than the average SIMS values obtained from two grains (13.0 ± 0.74‰). Note, that this
308 sample has a relatively large intra-grain-variability.
309
310 **In-situ oxygen isotope geochemistry of zircon**
311 Zircons are typically around 100 µm long, and less than 50 µm wide. CL imaging shows
312 magmatic rhythmic zoning. In the more than hundred zircons studied by our group (Leresche
313 2013; Nescher 2013; Seitz 2016), we have found only a few grains with xenocrystic cores (< 1
314 %), and none of the zircons from the samples investigated for this study has a xenocrystic core.
315 No metamorphic or late hydrothermal overgrowths were found. We obtained a total of 83
316 analyses from 67 grains, from 7 different flows and 1 ignimbrite (Tab. 2a). Figure 9 is a
317 composite of CL images of zircon from all 8 samples, with analysis spots and measured $\delta^{18}O$
318 shown.
319

Always consult and cite the final, published document. See http:/www.minsocam.org or GeoscienceWorld

The variation between individual zircon grains in any given sample are relatively large, up to 2.6 ‰ (Fig. 10). This is quite intriguing, and contrasts with the inter-grain homogeneity observed among quartz grains (in the same sample). Hence the zircons record a complex history for each sample. Zircons from sample rhyN7 (Laguna Sucia) exhibit the most pronounced variation seen in this study: a 2.6 ‰ range in $\delta^{18}O$ which corresponds to the full range in $\delta^{18}O$ from 7.5 ‰ to 10.1 ‰ here observed in one single sample. Nevertheless, the mean of its zircon population (8.7 ‰) is indistinguishable from those of other flows. Other samples show significant variation between zircon crystals as well, ranging from 0.8 ‰ to 1.7 ‰, but again samples are very similar in their arithmetic mean values of 8.5 ‰ to 8.8 ‰. The only ignimbrite sample has a slightly higher mean of 9.1 ‰. It has a similar inter-grain variation, from 7.7 ‰ to 9.8 ‰, despite the fact that only a small number of grains was analyzed. Interestingly, low values < 8.0 ‰ (from 7.5 ‰ to 7.9 ‰) as well as high values (9.1 - 10.1 ‰) are found in most samples.

The variability within single grains (Fig. 9 and Fig. 10), in contrast, is rather limited. In fact, where multiple analyses of a grain were carried out, the $\delta^{18}O$ values overlap within error, even where core respectively rim domains were targeted. Only sample rhyN7 has one zircon where the two spots analyzed are significantly different at a 2σ uncertainty level of 0.37 ‰. The core value is 8.4 ‰, while the rim value is 9.4 ‰.

Discussion

Assessment of oxygen isotope equilibrium between quartz, zircon, and whole rock

Isotopic equilibrium between two mineral phases can be evaluated in a $\delta^{18}O_A - \delta^{18}O_B$ plot (Taylor and Sheppard 1986). Figure 11 evaluates the state of equilibrium between quartz and

Always consult and cite the final, published document. See http:/www.minsocam.org or GeoscienceWorld

zircon and between quartz and whole rock. Quartz and zircon or quartz and whole rock pairs in equilibrium should plot along the line of equilibrium. The temperature range of minimum 700°C and maximum 900°C was chosen to cover the whole range of magmatic temperatures. For a detailed discussion of the crystallization temperature for quartz and zircon crystals see Seitz et al. 2018. The equilibrium fractionation factors used for Figure 11 are listed in Tab. 3.

There are several calibrations published for quartz-zircon, and probably the most commonly employed fractionation factors for $\Delta_{quartz\text{-}zircon}$ are from Zheng 1996, Valley 2003 and Trail et al. 2009. These fractionation factors vary between 2.5 ‰ and 3.3 ‰ at 700 C°, depending on the calibration chosen. In Fig. 11b the individual zircon $\delta^{18}O$ values are plotted against the average quartz $\delta^{18}O$ value of the corresponding sample. Even using the largest fractionation of 2.4 ‰ (900°C) and 3.3 ‰ (700 C°; Zheng 1996) the $\delta^{18}O_{quartz} - \delta^{18}O_{zircon}$ plot (Fig. 11b) highlights that most zircon crystals are not in high-temperature isotopic equilibrium with quartz. Only quartz and zircon from sample rhyPN73 plot between the equilibrium fractionation lines of 700°C and 900°C. The disequilibrium features shown in Fig. 11b are not surprising, since quartz values are homogeneous, and zircon $\delta^{18}O$ values show a large variability. A look at the ignimbrite sample ignSL75 illustrates this point: the measured $\Delta_{quart\text{-}zircon}$ fractionation ranges from 1.6 ‰ to 3.4 ‰. Most other samples show a similar range of fractionation. In the past, quartz-zircon disequilibrium was often attributed to late stage, hydrothermal alteration of quartz (e.g., King et al. 1997). In the present case, however, alteration of quartz is not likely due to the homogenous isotopic profiles measured and the preservation of igneous titanium zoning (Seitz 2016; Seitz et al. 2016b; Seitz et al. 2018; see additional discussion below). Alternatively, we need to consider that zircon, as accessory phase, and quartz might record very different aspects of the magmatic

Always consult and cite the final, published document. See http:/www.minsocam.org or GeoscienceWorld

366 evolution (Claiborne et al., 2010; Gualda and Ghiorso, 2013; Chamberlain et al. 2014; Till et al.
367 2016. Budd et al. 2017). In this sense, quartz-zircon disequilibrium reflects that zircons are
368 antecrysts derived from a heterogeneous source, as it has been proposed for the Yellowstone
369 magmatic system (e.g., Bindeman et al. 2008b; Wotzlaw et al. 2014), while quartz crystallized
370 later from their host magma.
371
372 The equilibrium $\delta^{18}O$ whole rock composition of rhyolitic rocks can be investigated by using a
373 quartz-rhyolite melt fractionation factor. The equilibrium fractionation $\Delta_{quartz\text{-}rhyolite}$ can be
374 calculated from $\Delta_{CO2\text{-}rhyolite}$ (Appora et al. 2003) and $\Delta_{CO2\text{-}quartz}$ (Zhao and Zheng 2003).
375 Depending on the temperature the fractionation varies between 0.5 ‰ (900°C) and 0.8 ‰
376 (700°C). Hence quartz-whole rock ^{18}O fractionation should be small, between 0.5 – 1.0 ‰ at
377 magmatic temperatures. The $\delta^{18}O_{quartz} - \delta^{18}O_{whole\ rock}$ plot in Fig. 11a reveals that this is not the
378 case. Especially for the ignimbrites, quartz and its whole rock are far from equilibrium at these
379 temperatures: the whole rocks show elevated oxygen isotope values of around 15.0 – 16.0 ‰ and
380 are thus substantially higher than the average 11.0 ‰ quartz values obtained from ignimbrites.
381 This observation is in agreement with the observed strong chemical and mineralogical alteration
382 in ignimbrites, which resulted in carbonate precipitation, and replacement of feldspar and mafic
383 minerals by hydrous minerals and carbonate. The high whole rock values, as well as the
384 replacement mineralogy clearly suggests a low temperature (<<500°C) alteration of these
385 ignimbrites. Therefore, whole rock values do not represent melt $\delta^{18}O$ values. The disequilibrium
386 is less pronounced for most flow samples. Quartz values are often, as expected, just slightly
387 higher than their whole rock or identical within error, i.e. they approach high temperature
388 equilibrium. However, there are also some samples where the whole rock value is more than 1.0

Always consult and cite the final, published document. See http:/www.minsocam.org or GeoscienceWorld

389 ‰ higher than the corresponding quartz value. Nevertheless, this shows that flows have been less
390 altered by hydrothermal fluids, as is also suggested by the petrography of these samples.
391
392 Most zircon crystals are not in equilibrium with the whole rock $\delta^{18}O$ composition (see Fig. S2 in
393 data repository). The fractionation obtained between zircon and whole rock suggests
394 unrealistically low equilibrium temperatures for most samples.
395
396 **Hydrothermal alteration**
397 The very high $\delta^{18}O$ whole rock values of ignimbrites and of some flows suggest that the rocks
398 were hydrothermally altered. This hydrothermal alteration, confirmed by carbonate and clay
399 mineral formation in the ignimbrite and some of the flows, occurred at relatively low
400 temperatures, in the stability field of carbonates and clays, typically expected to be below 300 -
401 400°C. This is not surprising, since it is known that whole rocks are prone to change during
402 hydrothermal alteration (Baumgartner and Valley 2001). Quartz has been shown to change its
403 isotopic composition (e.g., King et al. 1997; Bindeman and Valley 2002). In fact, many workers
404 suggest that only zircon preserves its original magmatic signature as it is highly resistant to
405 weathering, alteration and has an exceedingly slow diffusion (e.g., Valley 2003). However, the
406 CL data presented in Fig. 6 and Fig. 7 (see also Fig. S1 in data repository) clearly shows that the
407 quartz crystals did not recrystallize during alteration. They display igneous, mostly Ti-induced
408 CL-zoning (Seitz et al. 2016b; Seitz et al. 2018). In the present case, thus, exchange of ^{18}O
409 between quartz and fluids during hydrothermal interaction could only be due to diffusion as
410 opposed to dissolution-precipitation.
411

Always consult and cite the final, published document. See http:/www.minsocam.org or GeoscienceWorld

To explore the possibility of oxygen isotope re-equilibration in quartz via diffusion, we performed diffusion calculation modeling using the SIMS data. Across more than 600 data points for quartz by SIMS (Fig. 12a, Tab. 2b), compositions are homogeneous with consistently high values, with most analyses falling between 11.0 ‰ to 13.0 ‰. If grains were changed by diffusion during a hydrothermal event, diffusion needed to be sufficiently fast to completely homogenize the grains. Hence the diffusion distance needs to be much larger than half of the typical grain size (~1mm). A reasonable minimal distance is 500 µm. The required diffusion time, $t = 0.4\ a^2/D$ for a sphere with the grain radius a and the diffusion coefficient D. Bloch and Ganguly 2014 showed that this would result in a 98% re-equilibration of a sphere. The result is contoured in Fig. 13 for 500 µm. The water present diffusion coefficient of Giletti and Yund 1984 parallel to the c-axis of quartz was used to obtain a minimum time. This D compares well with the Dennis 1984 data. Diffusion in quartz is one to three orders faster parallel to the c-axis than perpendicular to it. We use the parallel diffusion coefficient of Giletti and Yund 1984 to obtain a minimum time estimate needed for re-equilibration, despite the fact that most quartz crystals were cut perpendicular to the c-axis. A re-equilibration time of more than $5*10^7$ yr is needed at 400°C and a duration of over $4*10^9$ yr is required at 300°C. Hence diffusive homogenization of quartz would take prohibitively long. Thus, a low temperature hydrothermal water-rock interaction cannot change quartz phenocryst compositions without recrystallisation, in agreement with our observations. Nevertheless, we interpret the – mostly subtle - changes in $\delta^{18}O$ measured close to cracks, embayments, and grain boundaries to reflect the effect of hydrothermal alteration. The half-with of the alteration is about 25 µm. This alteration distances would require roughly 125 ky at 400°C, a time span comparable to the life time of a hydrothermal system (Arehart et al. 2002; Rowland and Simmons 2012; Chiaradia et al. 2013).

Always consult and cite the final, published document. See http:/www.minsocam.org or GeoscienceWorld

In conclusion, the homogeneous $\delta^{18}O$ values of quartz are clearly magmatic in origin. Since diffusion of oxygen in zircon is even slower (Watson and Cherniak 1997; Cherniak and Watson 2003; Farver 2010), the above discussion also holds for the $\delta^{18}O$ composition of zircon, and zircon oxygen compositions should not be influenced by hydrothermal fluid-rock interaction, as long as they are not recrystallized.

Significance of $\delta^{18}O$ of quartz and zircon for magma evolution

Several of the quartzes from the flows and ignimbrites of the ELC were previously examined for their Ti-in-quartz zonation to derive timescales (Seitz et. al. 2016, Seitz et al. 2018). These studies determined short growth and residence times in the order of years to tens of years for these quartz crystals, based on the sharpness of Ti-zoning patterns measured by NanoSIMS. The extremely homogeneous profiles observed in quartz, as well as the negligible differences measured between grains could be the result of growth from a homogeneous magma or, alternatively, they could have been re-homogenized at magmatic temperatures. The latter seems to be unlikely, because the diffusion of Ti in quartz ($4.4*10^{-19}$ m^2/s, Cherniak et al. 2007) is very similar to that of oxygen self-diffusion in dry quartz ($6.3*10^{-19}$ m^2/s; Sharp et al. 1991) at magmatic temperatures (of 1000°C; see also Fig 13). Since very delicate Ti-zoning patterns are evident in CL-imaging, significant diffusion can be excluded. Hence, we argue that the $\delta^{18}O$ of quartz is a magmatic signature; its value reflecting the composition of the rhyolitic magma in the period of quartz crystal growth prior to eruption; this period is thought to be in the order of years to tens of years (Seitz et al. 2016, Seitz et al. 2018). The question is whether the small variations between the diverse flows reflect sampling of discrete magma reservoirs with subtle compositional differences or a systematic temporal evolution over time. At the moment we

Always consult and cite the final, published document. See http:/www.minsocam.org or GeoscienceWorld

458 cannot discern a systematic temporal evolution as has been observed for the Toba volcanic zone,
459 for example. Based on in-situ quartz data Budd et al. 2017 could identify an important addition
460 of a low-$\delta^{18}O$ component, i.e. hydrothermally altered rock, late in the genesis of the Toba
461 magmas.
462
463 The $\delta^{18}O$ in-situ analysis of the zircon crystals illustrate a large grain-to-grain variability, yet
464 zircon grains are not zoned; no xenocrystic cores are present. These observations suggests that
465 zircons are antecrysts (as defined by Miller et al. 2003), crystallizing from discrete magma
466 reservoirs with different oxygen isotope compositions or a heterogeneous magma body.
467 Subsequent magma movement – percolation and mixing – scooped up these zircons resulting in a
468 heterogeneous zircon population. Such a crystal cargo is well documented for many silicic
469 magma system (Gualda and Ghiorso 2013, Bindemann and Simakin 2014, Wotzlaw et al. 2014,
470 Bachmann and Huber 2016). Wotzlaw et al. 2014 explained the diverse $\delta^{18}O$ values of zircons
471 from Yellowstone by remelting an isotopically heterogeneous crust, where zircons crystallized
472 from different melt pods and then were accumulated together with the melt in a larger magma
473 chamber. The long-term assembly of the EQC magma with mantle and particularly crustal
474 contributions (see below) would be expected to result in a diverse crystal cargo, irrespective of
475 the exact origin of the high $\delta^{18}O$ crustal signature. However, at this point, we cannot determine
476 whether this diversity results from a heterogeneous source, an assembly of isolated magma
477 batches, or extraction of diverse zircons together with interstitial melt from a crustal mush.
478

479 **Evidence of crustal melting**

480 Both quartz and zircon reflect a magmatic isotope signature and are used here to discuss the
481 petrological and geological implications for the CAP, specifically the EQC, and its magma

Always consult and cite the final, published document. See http:/www.minsocam.org or GeoscienceWorld

source in the Chaltén area. In Fig. 14 the EQC volcanic rocks from the Chaltén area are compared to the large volcanic silicic systems worldwide. The melt composition of the EQC samples was calculated using minimum and maximum values of the quartz $\delta^{18}O$ composition for a temperature range of 700-900°C based on the Appora et al. 2003 and the Zhao and Zheng 2003 calibrations assuming equilibrium between quartz and a rhyolitic melt (see Tab. 3). The compilation in Fig. 14 highlights the particularity of our dataset. The EQC volcanic rocks are characterized by an exceptionally high SiO_2 and $\delta^{18}O$ composition, when compared to other large silicic systems such as the Fish Canyon Tuff, Central Snake River Plain or Great Basin Tuff in the western US (e.g., Folkes et al. 2013 and references therein). Other examples of high $\delta^{18}O$ rhyolites come from Karoo-Etendeka province (southern Africa), from the Altiplano-Puna Volcanic Complex and Cerro Galan (NW Argentina) and Tuscany (Italy) and from the Himalaya (Taylor and Turi 1976; France-Lanord et al. 1988; Masuda and O'Neil 1994; Barnekow 2000) and from the Caetano Tuff in Nevada, USA (Watts et al. 2016). The melting of a pre-existing, non-mafic (sedimentary, volcanic, granitic) crust is proposed to be important for the rhyolite formation in all these regions (Pichavant et al. 1988; Peccerillo 2017, see also Scaillet et al. 2016).

The importance of crustal melting in the formation of the CAP has been discussed by several papers in the past (Baker et al. 1981; Gust et al. 1985; Wever and Storey 1992; Pankhurst and Rapela 1995; Pankhurst et al. 1998; Riley et al. 2001). While early papers advocate crustal melting, later works suggest complex crystal fractionation and assimilation processes of a mafic crust. Only a few oxygen isotope data are available so far, and our contribution extends the data base considerably. The high $\delta^{18}O$ signatures the EQC flows and ignimbrites in the Chaltén

Always consult and cite the final, published document. See http:/www.minsocam.org or GeoscienceWorld

505 suggest a significant crustal - most likely sedimentary - contribution to the melt formation
506 process. Indeed, oxygen isotopes are an excellent tracer of a crustal signature, since the mantle is
507 homogeneous at 5.5 ‰ (Mattey et al. 1994). Zircons crystallized in equilibrium with a mantle
508 melt, should have $\delta^{18}O$ values around 5.3 ‰ (Valley 2003). Quartz $\delta^{18}O$ values from typical
509 rhyolites derived by simple closed system fractionation from a mafic parent range usually from 6
510 ‰ to 8 ‰ (Bindeman 2008). The high $\delta^{18}O$ signature of the EQC (zircon: 7.5 ‰ – 10.5 ‰,
511 quartz: 11 – 13 ‰) ties in very well with the peraluminous composition of these volcanic rocks,
512 a characteristic documented all over the CAP (e.g., Riley et al. 2001). The high oxygen isotope
513 signature suggests either a large amount of assimilation with a sedimentary or felsic component
514 or direct partial melting of a sedimentary or felsic source (e.g., carbonates: 20 - 30 ‰ and
515 siliciclastic sediments: 10 - 20 ‰; granitoids: 7 - 14 ‰; Kolodny and Epstein 1976; Arthur et al.
516 1983, see also compilation in Taylor and Sheppard 1986; Eiler 2001; Bindeman 2008). Both
517 scenarios – assimilation and melting – require a significant heat input (Annen and Sparks 2002;
518 Dufek and Bergantz 2005; Annen 2009; Whittington et al. 2009; Furlong and Chapman 2013).
519 Yet, it is evident that the observed signature cannot be achieved by simple models of fractional
520 crystallization – as closed system fractional crystallization produces small oxygen isotope
521 variation in the order of 1 ‰ – but clearly requires addition of sedimentary or felsic materials
522 (Taylor and Sheppard 1986; Chappell and White 1992; King and Valley 2001). Simple mass-
523 balance calculations suggest that ca. 50 % of a crustal material with a composition of $\delta^{18}O = 15$
524 ‰, which corresponds to a typical value of a paragneiss or meta-sandstone (compare Hoefs
525 2018) has to be added to a typical basaltic magma (with an $\delta^{18}O = 5.5$ ‰) to achieve the
526 observed high-$\delta^{18}O$ signature of the EQC ignimbrites and flows. Currently there are no oxygen
527 isotope analysis available for potential source rocks in the area, so the above calculations are a

Always consult and cite the final, published document. See http:/www.minsocam.org or GeoscienceWorld

528 first estimate. Higher or lower percentage of crustal contribution are needed respectively
529 depending on the composition of the composition of the actual crustal rocks involved.
530
531 The estimate agrees well with results from other high $\delta^{18}O$ regions (e.g. Puna, Karoo); these
532 studies discuss up to or in some cases more than 50 % of contamination to reach similarly high
533 oxygen isotope values. The Neogene ignimbrites of the Altiplano-Puna Volcanic Complex and
534 Cerro Galan in Argentina are long known for their high $\delta^{18}O$ signature with whole rocks value >
535 9 – 14 ‰ for rhyodacitic ignimbrites and 8 - 10 ‰ for basalts and andesites (Harmon et al. 1984;
536 Taylor 1986). Recent work (Kay et al. 2010; Folkes et al. 2013; Freymuth et al. 2015) using
537 quartz phenocrysts confirms this pattern; with values in the range from 8 – 10 ‰. They discuss
538 assimilation-fractional crystallization models, which suggest that the crustal melt proportion
539 acquired by these ignimbrite magmas is variable but high - on the order of 22 – 68 % (see also
540 Jones et al. 2015).
541

542 **Implications**

543 The unique dataset presented here demonstrates that the isotopic composition of quartz can be
544 used to characterize extrusive rocks, provided care is taken to demonstrate the absence of
545 recrystallization. Resetting quartz in low temperature hydrothermal systems through diffusion
546 requires millions of years (even at ca. 400°C). This time span is typically not available in
547 hydrothermal environments. We suggest that quartz can indeed preserves its magmatic oxygen
548 isotope signature. Quartz crystallized late during the evolution of the rhyolite magmas of the
549 EQC, recording the $\delta^{18}O$ composition of the erupted magma batch.
550

Always consult and cite the final, published document. See http:/www.minsocam.org or GeoscienceWorld

The zircon oxygen isotope record, on the other hand, rather reflects the overall, long-term evolution of the magmatic system. Most of the investigated zircons are antecrysts, which were accumulated in the magma reservoir during the evolution of the magmatic system. Thus, they likely capture information about the source region feeding the magma reservoir. Quartz in contrast will record the last stages of the magmatic system and thus might provide important information on the build-up and duration of magma chamber processes in the upper crust.

Quartz-zircon disequilibrium is commonly observed (see e.g., Bindeman and Simakin 2014). The data proves that in the case of the EQC volcanic rocks of the Chaltén area, this is not due to post-magmatic alteration of quartz. The homogeneity of quartz, the short crystallization time of quartz (Seitz et al. 2016b, Seitz et al. 2018), the zircon diversity and the disequilibrium between quartz and zircon clearly indicate that zircon and quartz growth was not contemporaneous. Indeed, equilibrium should not be expected. However, the causes of disequilibrium need to be examined, if we want to achieve a better understanding of the magmatic system and in particular when attempting thermometry.

It is now commonly accepted that major rock forming minerals like quartz, feldspar or hornblende and accessory phases like zircon record very different parts of the magmatic history (i.e., Claiborne et al., 2010; Gualda and Ghiorso, 2013; Chamberlain et al. 2014; Till et al. 2016). Our results from the Chaltén area and the data from Toba by Budd et al. 2017 underline the potential of investigating quartz, as its oxygen isotope signature can decipher magmatic processes that are not reflected in zircon record. The present work convincingly illustrates the complementing nature of quartz and zircon analysis, and thus the advantage of this approach.

Always consult and cite the final, published document. See http:/www.minsocam.org or GeoscienceWorld

574 SIMS techniques are now more readily available and they will allow us to gain a better
575 understanding of the texture and chemistry of quartz, an important rock forming mineral in
576 silicic systems. A detailed look at quartz is also interesting in combination with other in-situ
577 methods, which illustrate zonation of quartz, like Ti-diffusion chronometry (Wark et al. 2007;
578 Saunders et al. 2010; Matthews et al. 2012a; 2012b; Chamberlain et al. 2014; Seitz et al. 2016b;
579 Seitz et al. 2018).
580
581 The importance of crustal melting in the formation of the CAP, and other large silicic systems,
582 has been discussed controversially in the past, and our oxygen isotope data allow a new look at
583 this subject. We recognize that widespread crustal anatexis seems difficult to achieve due to the
584 high thermal energy required, yet the presented oxygen isotope data support partial melting of an
585 ^{18}O-rich crust to form the silicic volcanic rocks in the Chaltén area. A follow up study is in
586 progress - also using other tracers such as Sr or Pb isotopes, as well as high precision U-Pb
587 dating - to better quantify and model the crustal component. If the high $\delta^{18}O$ oxygen isotope
588 values prove to be a large-scale signature, suggested by the peraluminous character of the CAP
589 volcanic rocks, this has important consequence of how to discuss crustal melting and in turn how
590 to interpret the tectonic-magmatic models suggested for the CAP.
591

592 **Acknowledgements**

593 We thank the authorities of the Parque Nacional de los Glaciares (Argentina) for the permission
594 to sample and the rangers in El Chaltén for their support. A special thank you goes to A. Kosmal
595 (El Chaltén) for his hospitality, logistic support and geological insights. We also like to thank our
596 field assistants N. Buchs and E. May for their help. We thank P. Vonlanthen for the introduction

Always consult and cite the final, published document. See http:/www.minsocam.org or GeoscienceWorld

to the cathodoluminescence laboratory. We thank L. Caricchi and O. Müntener for helpful discussions. We appreciated the constructive suggestions by M. Stelten and L. Claiborne, which have led to a significant improvement of the manuscript. We gratefully acknowledge funding by the Swiss National Science Foundation (Fund 200020_150078 to BP, 200021_153094 to LPB) and PCI CASA funding of the Swiss government to LPB

References

Allan, M.M., and Yardley, B.W.D. (2007) Tracking meteoric infiltration into a magmatic-hydrothermal system: A cathodoluminescence, oxygen isotope and trace element study of quartz from Mt. Leyshon, Australia. Chemical Geology, 240, 343–360.

Angiboust, S., Hyppolito, T., Glodny, J., Cambeses, A., Garcia-Casco, A., Calderón, M., and Juliani, C. (2017) Hot subduction in the middle Jurassic and partial melting of oceanic crust in Chilean Patagonia. Gondwana Research, 42, 104–125.

Ankney, M.E., Bacon, C.R., Valley, J.W., Beard, B.L., and Johnson, C.M. (2017) Oxygen and U-Th isotopes and the timescales of hydrothermal exchange and melting in granitoid wall rocks at Mount Mazama, Crater Lake, Oregon. Geochimica et Cosmochimica Acta, 213, 137–154.

Annen, C. (2009) From plutons to magma chambers: Thermal constraints on the accumulation of eruptible silicic magma in the upper crust. Earth and Planetary Science Letters, 284, 409–416.

Annen, C., and Sparks, R.S.J. (2002) Effects of repetitive emplacement of basaltic intrusions on thermal evolution and melt generation in the crust. Earth and Planetary Science Letters, 203, 937–955.

Appleby, S.K., Gillespie, M.R., Graham, C.M., Hinton, R.W., Oliver, G.J.H., and Kelly, N.M. (2010) Do S-type granites commonly sample infracrustal sources? New results from an integrated O, U–Pb and Hf isotope study of zircon. Contributions to Mineralogy and Petrology, 160, 115–132.

Appora, I., Eiler, J.M., Matthews, A., and Stolper, E.M. (2003) Experimental determination of oxygen isotope fractionations between CO2 vapor and soda-melilite melt. Geochimica et Cosmochimica Acta, 67, 459–471.

Arehart, G.B., Christenson, B.W., Wood, C.P., Foland, K.A., and Browne, P.R.L. (2002) Timing of volcanic, plutonic and geothermal activity at Ngatamariki, New Zealand. Journal of Volcanology and Geothermal Research, 116, 201–214.

Always consult and cite the final, published document. See http:/www.minsocam.org or GeoscienceWorld

630 Arthur, M.A., Anderson, T.F. and Kaplan, I.R. (1983) Stable isotopes in sedimentary geology.
631 SEPM Short Course 10: 432 p.

632 Baker, P.E., Rea, W.J., Skarmeta, J., Caminos, R., and Rex, D.C. (1981) Igneous History of the
633 Andean Cordillera and Patagonian Plateau around Latitude 46 degrees S. Philosophical
634 Transactions of the Royal Society A: Mathematical, Physical and Engineering Sciences, 303,
635 105–149.

636 Barnekow, P. (2000) Volcanic rocks from central Italy: an oxygen isotopic microanalytical and
637 geochemical study, Ph.D. thesis University Göttingen, Göttingen.

638 Baumgartner, L.P., and Valley, J.W. (2001) Stable Isotope Transport and Contact Metamorphic
639 Fluid Flow. Reviews in Mineralogy and Geochemistry, 43, 415–467.

640 Benedini, L., Gregori, D., Strazzere, L., Falco, J.I., and Dristas, J.A. (2014) Lower Pliensbachian
641 caldera volcanism in high-obliquity rift systems in the western North Patagonian Massif,
642 Argentina. Journal of South American Earth Sciences, 56, 1–19.

643 Bindeman, I. (2008) Oxygen Isotopes in Mantle and Crustal Magmas as Revealed by Single
644 Crystal Analysis. Reviews in Mineralogy and Geochemistry, 69, 445–478.

645 Bindeman, I.N., Fu, B., Kita, N.T., and Valley, J.W. (2008b) Origin and Evolution of Silicic
646 Magmatism at Yellowstone Based on Ion Microprobe Analysis of Isotopically Zoned
647 Zircons. Journal of Petrology, 49(1), 163–193.

648 Bindeman, I.N., and Simakin, A.G. (2014) Rhyolites—Hard to produce, but easy to recycle and
649 sequester: Integrating microgeochemical observations and numerical models. Geosphere, 10,
650 930–957.

651 Bindeman, I.N., and Valley, J.W. (2002) Oxygen isotope study of the Long Valley magma
652 system, California: isotope thermometry and convection in large silicic magma bodies.
653 Contributions to Mineralogy and Petrology, 144, 185–205.

654 Bindeman, I.N., and Valley, J.W. (2001) Low-delta18O Rhyolites from Yellowstone: Magmatic
655 Evolution Based on Analyses of Zircons and Individual Phenocrysts. Journal of Petrology,
656 42(8), 1491–1517.

657 Bindeman, I.N., Ponomareva, V.V., Bailey, J.C., and Valley, J.W. (2004) Volcanic arc of
658 Kamchatka: a province with high-δ18O magma sources and large-scale 18O/16O depletion
659 of the upper crust. Geochimica et Cosmochimica Acta, 68, 841–865.

660 Bloch, E., and Ganguly, J. (2014). 176Lu–176Hf and 147Sm–143Nd ages of the Martian
661 shergottites: Evaluation of the shock-resetting hypothesis through diffusion kinetic
662 experiments and modeling, and petrological observations. Earth and Planetary Science
663 Letters, 395(C), 173–183.

664 Bouhier, V.E., Franchini, M.B., Caffe, P.J., Maydagán, L., Rapela, C.W., and Paolini, M. (2017)
665 Petrogenesis of volcanic rocks that host the world-class Ag─Pb Navidad District, North

Always consult and cite the final, published document. See http:/www.minsocam.org or GeoscienceWorld

666 Patagonian Massif: Comparison with the Jurassic Chon Aike Volcanic Province of
667 Patagonia, Argentina. Journal of Volcanology and Geothermal Research, 338, 101–120.

668 Bowman, J.R., Moser, D.E., Valley, J.W., Wooden, J.L., Kita, N.T., and Mazdab, F.K. (2012)
669 Zircon U-Pb isotope, 18O and trace element response to 80 m.y. of high temperature
670 metamorphism in the lower crust: Sluggish diffusion and new records of Archean craton
671 formation. American Journal of Science, 311, 719–772.

672 Bryan, S.E., and Ferrari, L. (2013) Large igneous provinces and silicic large igneous provinces:
673 Progress in our understanding over the last 25 years. Geological Society of America
674 Bulletin, 125, 1053–1078.

675 Bryan, S.E., Riley, T.R., and Jerram, D.A. (2002) Silicic volcanism: an undervalued component
676 of large igneous provinces and volcanic rifted margins. Geological Society of America,
677 Special Paper, 362.

678 Budd, D.A., Troll, V.R., Deegan, F.M., Jolis, E.M., Smith, V.C., Whitehouse, M.J., Harris, C.,
679 Freda, C., Hilton, D.R., Halldórsson, S.A., and Bindeman, I.N. (2017) Magma reservoir
680 dynamics at Toba caldera, Indonesia, recorded by oxygen isotope zoning in quartz, 1–11.

681 Chamberlain, K.J., Morgan, D.J., and Wilson, C.J.N. (2014) Timescales of mixing and
682 mobilisation in the Bishop Tuff magma body: perspectives from diffusion chronometry.
683 Contributions to Mineralogy and Petrology, 168.

684 Chappell, B.W., and White, A.J.R. (1992) I- and S-type granites in the Lachlan Fold Belt.
685 Transactions of the Royal Society of Edinburgh: Earth Sciences, 83, 1–26.

686 Cherniak, D.J., Watson, E.B., and Wark, D.A. (2007) Ti diffusion in quartz. Chemical Geology,
687 236, 65–74.

688 Cherniak, D.J., and Watson, E.B. (2003) Diffusion in Zircon. Reviews in Mineralogy and
689 Geochemistry, 53(1), 113–143.

690 Chiaradia, M., Schaltegger, U., Spikings, R., Wotzlaw, J.-F., and Ovtcharova, M. (2013) How
691 Accurately Can We Date the Duration of Magmatic-Hydrothermal Events in Porphyry
692 Systems? — An Invited Paper. Economic Geology, 108, 565–584.

693 Claiborne, L.L., Miller, C.F., Flanagan, D.M., Clynne, M.A., and Wooden, J.L. (2010) Zircon
694 reveals protracted magma storage and recycling beneath Mount St. Helens. Geology, 38(11),
695 1011–1014.

696 Coplen, T.B., Kendall, C., and Hopple, J. (1983) Comparison of stable isotope reference
697 samples. Nature, 302, 236–238.

698 Dennis, P.F. (1984) Oxygen self-diffusion in quartz under hydrothermal conditions. Journal of
699 Geophysical Research: Solid Earth, 89, 4047–4057.

700 Dopico, C.I.M.N., de Luchi, M.G.L., Rapalini, A.E., Wemmer, K., Fanning, C.M., and Basei,

Always consult and cite the final, published document. See http:/www.minsocam.org or GeoscienceWorld

M.A.S. (2017) Emplacement and temporal constraints of the Gondwanan intrusive complexes of northern Patagonia: La Esperanza plutono-volcanic case. Tectonophysics, 712-713, 249–269.

Dufek, J., and Bergantz, G.W. (2005) Lower Crustal Magma Genesis and Preservation: a Stochastic Framework for the Evaluation of Basalt–Crust Interaction. Journal of Petrology, 46, 2167–2195.

Eiler, J., Stolper, E.M., and McCanta, M.C. (2011) Intra- and Intercrystalline Oxygen Isotope Variations in Minerals from Basalts and Peridotites. Journal of Petrology, 52, 1393–1413.

Eiler, J.M. (2001) Oxygen Isotope Variations of Basaltic Lavas and Upper Mantle Rocks. Reviews in Mineralogy and Geochemistry, 43, 319–364.

Ellis, B.S., Szymanowski, D., Wotzlaw, J.F., Schmitt, A.K., Bindeman, I.N., Troch, J., Harris, C., Bachmann, O., and Guillong, M. (2017) Post-caldera Volcanism at the Heise Volcanic Field: Implications for Petrogenetic Models. Journal of Petrology, 58(1), 115–136.

Farver, J.R. (2010) Oxygen and Hydrogen Diffusion in Minerals. Reviews in Mineralogy and Geochemistry, 72(1), 447–507.

Fekete, S., Weis, P., Driesner, T., Bouvier, A.-S., Baumgartner, L.P., and Heinrich, C.A. (2016) Contrasting hydrological processes of meteoric water incursion during magmatic–hydrothermal ore deposition: An oxygen isotope study by ion microprobe. Earth and Planetary Science Letters, 451, 263–271.

Fildani, A., and Hessler, A.M. (2005) Stratigraphic record across a retroarc basin inversion: Rocas Verdes–Magallanes Basin, Patagonian Andes, Chile. Geological Society of America Bulletin, 117, 1596.

Folkes, C.B., de Silva, S.L., Bindeman, I.N., and Cas, R.A.F. (2013) Tectonic and climate history influence the geochemistry of large-volume silicic magmas: New δ18O data from the Central Andes with comparison to N America and Kamchatka. Journal of Volcanology and Geothermal Research, 262, 90–103.

Fourie, D.S., and Harris, C. (2011) O-isotope Study of the Bushveld Complex Granites and Granophyres: Constraints on Source Composition, and Assimilation. Journal of Petrology, 52(11), 2221–2242.

France-Lanord, C., Sheppard, S.M.F., and Fort, P.L. (1988) Hydrogen and oxygen isotope variations in the high himalaya peraluminous Manaslu leucogranite: Evidence for heterogeneous sedimentary source. Geochimica et Cosmochimica Acta, 52, 513–526.

Freymuth, H., Brandmeier, M., and Wörner, G. (2015) The origin and crust/mantle mass balance of Central Andean ignimbrite magmatism constrained by oxygen and strontium isotopes and erupted volumes. Contributions to Mineralogy and Petrology, 169, 58.

Furlong, K.P., and Chapman, D.S. (2013) Heat Flow, Heat Generation, and the Thermal State of

Always consult and cite the final, published document. See http:/www.minsocam.org or GeoscienceWorld

737 the Lithosphere. Annual Review of Earth and Planetary Sciences, 41, 385–410.

738 Giese, J., Seward, D., Stuart, F.M., Wüthrich, E., Gnos, E., Kurz, D., Eggenberger, U., and
739 Schreurs, G. (2010) Electrodynamic Disaggregation: Does it Affect Apatite Fission-Track
740 and (U-Th)/He Analyses? Geostandards and Geoanalytical Research, 34, 39–48.

741 Giletti, B.J., and Yund, R.A. (1984) Oxygen diffusion in quartz. Journal of Geophysical
742 Research: Solid Earth, 89, 4039–4046.

743 Grunder, A.L., and Wickham, S. (1991). Homogenization and lowering of 18O/16O in mid-
744 crustal rocks during extension-related magmatism in eastern Nevada. Earth and Planetary
745 Sciences Letters, 107, 416–431.

746 Gualda, G., and Ghiorso, M.S. (2013). The Bishop Tuff giant magma body: an alternative to the
747 Standard Model. Contributions to Mineralogy and Petrology, 166(3), 755–775.

748 Gualda, G., Pamukcu, A.S., and Ghiorso, M.S. (2012) Timescales of quartz crystallization and
749 the longevity of the Bishop giant magma body. PLoS ONE.

750 Gust, D.A., Biddle, K.T., Phelps, D.W., and Uliana, M.A. (1985) Associated middle to late
751 Jurassic volcanism and extension in southern South America. Tectonophysics, 116, 223–253.

752 Harmon, R.S., Barreiro, B.A., Moorbath, S., Hoefs, J., Francis, P.W., Thorpe, R.S., Deruelle, B.,
753 McHugh, J., and Viglino, J.A. (1984) Regional O-, Sr-, and Pb-isotope relationships in late
754 Cenozoic calc-alkaline lavas of the Andean Cordillera. Journal of the Geological Society,
755 141, 803–822.

756 Hervé, F., Calderón, M., Massonne, H.J., and Theye, T. (2007a) Metamorphic P-T conditions of
757 Late Jurassic rhyolites in the Magallanes fold and thrust belt, Patagonian Andes, Chile.
758 Journal of Iberian Geology, 33, 5 – 16.

759 Hervé, F., Pankhurst, R.J., Fanning, C.M., Calderón, M., and Yaxley, G.M. (2007b) The South
760 Patagonian batholith: 150 my of granite magmatism on a plate margin. Lithos, 97, 373–394.

761 Hoefs, J. (2018) Variations of Stable Isotope Ratios in Nature. In J. Hoefs, Ed., Stable Isotope
762 Geochemistry pp. 229–432. Springer International Publishing, Cham.

763 Huang, R., and Audétat, A. (2012) The titanium-in-quartz (TitaniQ) thermobarometer: A critical
764 examination and re-calibration. Geochimica et Cosmochimica Acta, 84, 75–89.

765 Japas, M.S., Sruoga, P., Kleiman, L.E., Gayone, M.R., Maloberti, A., and Comito, O. (2013)
766 Cinemática de la extensión jurásica vinculada a la Provincia Silícea Chon Aike, Santa Cruz,
767 Argentina. Revista de la Asociación Geologica Argentina, 70, 16–30.

768 Jones, R.E., Kirstein, L.A., Kasemann, S.A., Dhuime, B., Elliott, T., Litvak, V.D., Alonso, R.,
769 and Hinton, R. (2015) Geodynamic controls on the contamination of Cenozoic arc magmas
770 in the southern Central Andes: Insights from the O and Hf isotopic composition of zircon.
771 Geochimica et Cosmochimica Acta, 164, 386–402.

Always consult and cite the final, published document. See http:/www.minsocam.org or GeoscienceWorld

Kay, S.M., Coira, B.L., Caffe, P.J., and Chen, C.-H. (2010) Regional chemical diversity, crustal and mantle sources and evolution of central Andean Puna plateau ignimbrites. Journal of Volcanology and Geothermal Research, 198, 81–111.

Kay, S.M., Ramos, V.A., Mpodozis, C., and Sruoga, P. (1989) Late Paleozoic to Jurassic silicic magmatism at the Gondwana margin: Analogy to the Middle Proterozoic in North America? Geology, 17, 324–328.

King, E.M., and Valley, J.W. (2001) The source, magmatic contamination, and alteration of the Idaho batholith. Contributions to Mineralogy and Petrology, 142, 72–88.

King, E.M., Barrie, C.T., and Valley, J.W. (1997) Hydrothermal alteration of oxygen isotope ratios in quartz phenocrysts, Kidd Creek mine, Ontario: magmatic values are preserved in zircon. Geology, 25, 1079–1082.

Kolodny, Y., and Epstein, S. (1976) Stable isotope geochemistry of deep sea cherts. Geochimica et Cosmochimica Acta, 40, 1195–1209.

Lacroix, B., and Vennemann, T. (2015) Empirical calibration of the oxygen isotope fractionation between quartz and Fe–Mg-chlorite. Geochimica et Cosmochimica Acta, 149, 21–31.

Leresche, S. (2013) Etude structurale, géochimique, géochronologique et pétrographique d'une partie des roches encaissantes à l'Est de l'intrusionn du Mt. Fitz Roy (Patagonie, Argentine), 111 p. Master thesis, Universié de Lausanne, Lausanne.

Li, X.-H., Long, W.G., Li, Q.-L., Liu, Y., Zheng, Y.F., Yang, Y.-H., Chamberlain, K.R., Wan, D.F., Guo, C.H., Wang, X.C., and others (2010) Penglai Zircon Megacrysts: A Potential New Working Reference Material for Microbeam Determination of Hf–O Isotopes and U–Pb Age. Geostandards and Geoanalytical Research, 34, 117–134.

Malkowski, M., Schwartz, T., and Sickmann, Z. (2015) Jurassic–Cretaceous Stratigraphic Evolution of the Magallanes– Austral Deep-Water Foreland Basin, Argentine Patagonia, 1–64.

Manzini, M., Bouvier, A.-S., Baumgartner, L.P., Müntener, O., Rose-Koga, E.F., Schiano, P., Escrig, S., Meibom, A., and Shimizu, N. (2017) Weekly to monthly time scale of melt inclusion entrapment prior to eruption recorded by phosphorus distribution in olivine from mid-ocean ridges. Geology, 45, 1059–1062.

Masuda, H., and O'Neil, J.R. (1994) Oxygen isotope heterogeneity of phenocrysts in rhyolite from San Vincenzo, Italy, by laser microprobe analysis TI . Geochemical Journal, 28, 377–385.

Mattey, D., Lowry, D., and Macpherson, C. (1994) Oxygen isotope composition of mantle peridotite. Earth and Planetary Science Letters, 128, 231–241.

Matthews, N.E., Huber, C., Pyle, D.M., and Smith, V.C. (2012a) Timescales of Magma Recharge and Reactivation of Large Silicic Systems from Ti Diffusion in Quartz. Journal of

Always consult and cite the final, published document. See http:/www.minsocam.org or GeoscienceWorld

Petrology, 53, 1385–1416.

Matthews, N.E., Pyle, D.M., Smith, V.C., Wilson, C.J.N., Huber, C., and van Hinsberg, V. (2012b) Quartz zoning and the pre-eruptive evolution of the ~340-ka Whakamaru magma systems, New Zealand. Contributions to Mineralogy and Petrology, 163, 87–107.

Miller, C.F., McDowell, S.M., and Mapes, R.W. (2003) Hot and cold granites? Implications of zircon saturation temperatures and preservation of inheritance. Geology, 31, 529–532.

Mpodozis, C., and Ramos, V.A. (2008) Jurassic tectonics in Argentina and Chile: Extension, oblique subduction, rifting, drift and collisions? Revista de la Asociación Geologica Argentina, 63, 481–497.

Navarrete, C., Gianni, G., Echaurren, A., Kingler, F.L., and Folguera, A. (2016) Episodic Jurassic to Lower Cretaceous intraplate compression in Central Patagonia during Gondwana breakup. Journal of Geodynamics, 102, 185–201.

Nescher, P. (2013) Petrography, structural geology, geochemistry and metamorphism of the rocks in the eastern Fitz Roy foothills in Patagonia, Argentina, 155 p. Master thesis, Universtité de Lausanne, Lausanne.

Pankhurst, R.J., Schaefer, B.F., and Betts, P.G. (2011) Geodynamics of rapid voluminous felsic magmatism through time. Lithos, 123, 92–101.

Pankhurst, R.J., and Rapela, C.R. (1995) Production of Jurassic rhyolite by anatexis of the lower crust of Patagonia. Earth and Planetary Sciences Letters, 134, 23–36.

Pankhurst, R.J., Leat, P.T., Sruoga, P., Rapela, C.W., Márquez, M., Storey, B.C., and Riley, T.R. (1998) The Chon Aike province of Patagonia and related rocks in West Antarctica: A silicic large igneous province. Journal of Volcanology and Geothermal Research, 81, 113–136.

Pankhurst, R.J., Riley, T.R., Fanning, C.M., and Kelley, S.P. (2000) Episodic silicic volcanism in Patagonia and the Antarctic Peninsula: chronology of magmatism associated with the break-up of Gondwana. Journal of Petrology, 41, 605–625.

Peccerillo, A. (2017) Cenozoic Volcanism in the Tyrrhenian Sea Region, 2nd ed., 400 p. pp. XX–399. Springer International Publishing.

Pichavant, M., Kontak, D.J., Briqueu, L., Herrera, J.V., and Clark, A.H. (1988) The Miocene-Pliocene Macusani Volcanics, SE Peru. Contributions to Mineralogy and Petrology, 100, 325–338.

Ramírez de Arellano, C. (2011) Petrology and chemistry of the Chaltén Plutonic Complex and implications on the magmatic and tectonic evolution of the Southernmost Andes (Patagonia) during the Miocene, 154 p. Ph.D. thesis, Université de Lausanne, Lausanne.

Ramírez de Arellano, C., Putlitz, B., Müntener, O., and Ovtcharova, M. (2012) High precision U/Pb zircon dating of the Chaltén Plutonic Complex (Cerro Fitz Roy, Patagonia) and its

Always consult and cite the final, published document. See http:/www.minsocam.org or GeoscienceWorld

relationship to arc migration in the southernmost Andes. Tectonics, 31.

Riley, T.R., and Knight, K.B. (2001) Age of Pre-Break-Up Gondwana Magmatism. Antarctic Science, 13, 99–110.

Riley, T.R., and Leat, P.T. (1999) Large volume silicic volcanism along the proto-Pacific margin of Gondwana: lithological and stratigraphical investigations from the Antarctic Peninsula. Geological Magazine.

Riley, T.R., Flowerdew, M.J., Hunter, M.A., and Whitehouse, M.J. (2010) Middle Jurassic rhyolite volcanism of eastern Graham Land, Antarctic Peninsula: age correlations and stratigraphic relationships. Geol. Mag., 147, 581–595.

Riley, T.R., Leat, P.T., Pankhurst, R.J., and Harris, C. (2001) Origins of large volume rhyolitic volcanism in the Antarctic Peninsula and Patagonia by crustal melting. Journal of Petrology, 42, 1043–1065.

Riley, T.R., Millar, I.L., Watkys, M.K., Curtis, M.L., Leat, P.T., Klausen, M.B., and Fanning, C.M. (2004) U–Pb zircon (SHRIMP) ages for the Lebombo rhyolites, South Africa: refining the duration of Karoo volcanism. Journal of the Geological Society, 161, 547–550.

Rowland, J.V., and Simmons, S.F. (2012) Hydrologic, Magmatic, and Tectonic Controls on Hydrothermal Flow, Taupo Volcanic Zone, New Zealand: Implications for the Formation of Epithermal Vein Deposits. Economic Geology, 107, 427–457.

Saunders, K.E., Morgan, D.J., Baker, J.A., and Wysoczanski, R.J. (2010) The Magmatic Evolution of the Whakamaru Supereruption, New Zealand, Constrained by a Microanalytical Study of Plagioclase and Quartz. Journal of Petrology, 51, 2465–2488.

Scaillet, B., Holtz, F., and Pichavant, M. (2016) Experimental Constraints on the Formation of Silicic Magmas. Elements, 12, 109–114.

Seitz, S. (2016) Oxygen isotope data and constraints on magmatic timescales from the Chon Aike Province (Patagonia, Argentina), 211 p. Ph.D. thesis, Université de Lausanne, Lausanne.

Seitz, S., Putlitz, P., Baumgartner, L.P., Meibom, A., Escrig, S. and Bouvier, A.-S. (2018) A NanoSIMS Investigation on Timescales Recorded in Volcanic Quartz from the Silicic Chon Aike Province (Patagonia). Front. Earth Sci. 6:95.

Seitz, S., Baumgartner, L.P., Bouvier, A.-S., Putlitz, B., and Vennemann, T. (2016a) Quartz Reference Materials for Oxygen Isotope Analysis by SIMS. Geostandards and Geoanalytical Research, 41, 69–75.

Seitz, S., Putlitz, B., Baumgartner, L.P., Escrig, S., Meibom, A., and Bouvier, A.-S. (2016b) Short magmatic residence times of quartz phenocrysts in Patagonian rhyolites associated with Gondwana breakup. Geology, 44, 67–70.

Always consult and cite the final, published document. See http:/www.minsocam.org or GeoscienceWorld

878 Sharp, Z.D., Giletti, B.J., and Yoder, H.S. (1991) Oxygen diffusion rates in quartz exchanged
879 with CO2. Earth and Planetary Science Letters, 107, 339–348.

880 Skora, S., Baumgartner, L.P., Mahlen, N.J., Johnson, C.M., Pilet, S., and Hellebrand, E. (2006)
881 Diffusion-limited REE uptake by eclogite garnets and its consequences for Lu–Hf and Sm–
882 Nd geochronology. Contributions to Mineralogy and Petrology, 152(6), 703–720.

883 Sruoga, P., Japas, M.S., Salani, F.M., and Kleiman, L.E. (2014) La Peligrosa caldera (47° 15′S,
884 71° 40′W): A key event during the Jurassic ignimbrite flare-up in Southern Patagonia,
885 Argentina. Journal of Volcanology and Geothermal Research, 269, 44–56.

886 Tanner, D., Henley, R.W., Mavrogenes, J.A., and Holden, P. (2013) Combining in situ isotopic,
887 trace element and textural analyses of quartz from four magmatic-hydrothermal ore deposits.
888 Contributions to Mineralogy and Petrology, 166, 1119–1142.

889 Taylor, H.P. (1986) Igneous rocks; II, Isotopic case studies of Circumpacific magmatism.
890 Reviews in Mineralogy and Geochemistry, 16, 273–317.

891 Taylor, H.P., and Sheppard, S.M.F. (1986) Igneous rocks; I, Processes of isotopic fractionation
892 and isotope systematics. Reviews in Mineralogy and Geochemistry, 16, 227–271.

893 Taylor, H.P., and Turi, B. (1976) High-18/16O igneous rocks from the Tuscan Magmatic
894 Province, Italy. Contributions to Mineralogy and Petrology, 55, 33–54.

895 Thomas, J.B., Bruce Watson, E., Spear, F.S., Shemella, P.T., Nayak, S.K., and Lanzirotti, A.
896 (2010) TitaniQ under pressure: the effect of pressure and temperature on the solubility of Ti
897 in quartz. Contributions to Mineralogy and Petrology, 160, 743–759.

898 Trail, D., Bindeman, I.N., Watson, E.B., and Schmitt, A.K. (2009) Experimental calibration of
899 oxygen isotope fractionation between quartz and zircon. Geochimica et Cosmochimica Acta,
900 73, 7110–7126.

901 Valley, J.W. (2003) Oxygen isotopes in zircon. Reviews in Mineralogy and Geochemistry.

902 Valley, J.W., and Graham, C.M. (1996) Ion microprobe analysis of oxygen isotope ratios in
903 quartz from Skye granite: healed micro-cracks, fluid flow, and hydrothermal exchange.
904 Contributions to Mineralogy and Petrology, 124, 225–234.

905 Wang, Z., and Eiler, J. (2008) Insights into the origin of low-δ18O basaltic magmas in Hawaii
906 revealed from in situ measurements of oxygen isotope compositions of olivines. Earth and
907 Planetary Science Letters, 269, 377–387.

908 Wark, D.A., and Spear, F.S. (2005) Ti in quartz: Cathodoluminescence and thermometry.
909 Geochimica et Cosmochimica Acta Supplement, 69, 592.

910 Wark, D.A., and Watson, E.B. (2006) TitaniQ: a titanium-in-quartz geothermometer.
911 Contributions to Mineralogy and Petrology, 152, 743–754.

Always consult and cite the final, published document. See http:/www.minsocam.org or GeoscienceWorld

912 Wark, D.A., Hildreth, W., Spear, F.S., Cherniak, D.J., and Watson, E.B. (2007) Pre-eruption
913 recharge of the Bishop magma system. Geology, 35, 235.

914 Watson, E.B., and Cherniak, D.J. (1997) Oxygen diffusion in zircon. Earth and Planetary
915 Science Letters, 148(3-4), 527–544.

916 Watts, K.E., John, D.A., Colgan, J.P., Henry, C.D., Bindeman, I.N., and Schmitt, A.K. (2016).
917 Probing the Volcanic–Plutonic Connection and the Genesis of Crystal-rich Rhyolite in a
918 Deeply Dissected Supervolcano in the Nevada Great Basin: Source of the Late Eocene
919 Caetano Tuff. Journal of Petrology, 57(8), 1599–1644.

920 Watts, K.E., Bindeman, I.N., and Schmitt, A.K. (2011) Large-volume Rhyolite Genesis in
921 Caldera Complexes of the Snake River Plain: Insights from the Kilgore Tuff of the Heise
922 Volcanic Field, Idaho, with Comparison to Yellowstone and Bruneau-Jarbidge Rhyolites.
923 Journal of Petrology, 52, 857–890.

924 Wever, H.E., and Storey, B.C. (1992) Bimodal magmatism in northeast Palmer Land, Antarctic
925 Peninsula: Geochemical evidence for a Jurassic ensialic back-arc basin. Tectonophysics,
926 205, 239–259.

927 Whittington, A.G., Hofmeister, A.M., and Nabelek, P.I. (2009) Temperature-dependent thermal
928 diffusivity of the Earth's crust and implications for magmatism. Nature, 458, 319–321.

929 Wotzlaw, J.-F., Bindeman, I.N., Watts, K.E., Schmitt, A.K., Caricchi, L., & Schaltegger, U.
930 (2014) Linking rapid magma reservoir assembly and eruption trigger mechanisms at evolved
931 Yellowstone-type supervolcanoes. Geology, 42(9), 807–810.

932 Zhao, Z.-F., and Zheng, Y.F. (2003) Calculation of oxygen isotope fractionation in magmatic
933 rocks. Chemical Geology, 193, 59–80.

934 Zheng, Y.-F. (1993) Calculation of oxygen isotope fractionation in anhydrous silicate minerals.
935 Geochimica et Cosmochimica Acta, 57, 1079–1091.

936

937

938

939

940

941

942

943

Always consult and cite the final, published document. See http:/www.minsocam.org or GeoscienceWorld

Figure 1. Map of Patagonia showing the main outcrop areas of the Jurassic Chon Aike Province. The 175 Ma and 160 Ma contour line is separating the V1, V2 and V3 volcanic episode of the Chon Aike Porvince. Also shown are the Patagonian Batholith and the Patagonian Plateau Basalts (after Pankhurst et al. 1998; Hervé et al. 2007a). The study area is in the vicinity of the Miocene Chaltén Plutonic Complex.

Figure 2. Detailed geological map of the study area indicating the main sample locations Cerro (Co.) Madsen, Laguna Sucia, Half Moon, Loma de las Pizarras and Cerro (Co.) Polo (modified from Ramírez de Arellano et al. 2012; Leresche 2013 and Nescher2013).

Figure 3. (a) Overview photo of a rhyolitic lava dome (Half Moon) and flow (Lomo de las Pizarras) of the El Quemado Complex inter-folded with the Cretaceous pelitic sedimentary rocks of the Rio Mayer Formation. **(b)** Rhyolite showing magmatic flow banding and vesicles. For scale, the diameter of the hand lens is ~1.5 cm.

Figure 4. (a) Photo of multiple deposits of rhyolitic ignimbrites at Cerro (Co.) Polo. They discordantly overlying the Paleozoic clastic sequence of the Bahia de la Lancha Formation. Some ignimbrites contain volcanic bombs **(b)** and they often show lithic fragments and fiamme structures **(c)**. For scale, the head of the hammer is ~10 cm long.

Figure 5. Total alkali versus silica diagram of the El Quemado Complex in orange (this study). The shaded area is interpreted to result from alkali leaching and carbonate precipitation during hydrothermal alteration. Data from the literature for the Chon Aike Province, including the El Quemado Complex, are from Pankhurst and Rapela 1995; Pankhurst et al. 1998. R – rhyolite; D – dacite; TD – trachydacite; A – Andesite; TA – trachyandesite; BA – basaltic andesite; BTA – basaltic trachyandesite; B – basalt; TB – trachybasalt.

Always consult and cite the final, published document. See http:/www.minsocam.org or GeoscienceWorld

977 **Figure 6.** Cathodoluminescence images of quartz phenocrysts from rhyolitic lava flows, with
978 indicated SIMS analysis profiles. The white circles indicate the location of the $\delta^{18}O$ SIMS
979 analysis. The corresponding quartz profiles are shown in the panel below. The error bars
980 represent 2σ of the SIMS analysis. Open symbols are measured in cracks. The dotted line
981 represents major zones in CL.

982 **Figure 7.** Cathodoluminescence images of quartz phenocrysts from rhyolitic ignimbrites and
983 SIMS analysis profiles. The white dots indicate the location of the $\delta^{18}O$ SIMS analysis. The
984 corresponding quartz profiles are shown in the panel below. The error bars represent 2σ of
985 the SIMS analysis. Open symbols are measured in cracks. The dotted line represents major
986 zones in CL.

987 **Figure 8.** $\delta^{18}O$ SIMS analysis measured on quartz crystals from rhyolitic flows (orange) and
988 ignimbrites (green). The error bars represent 2σ of the SIMS analysis. Open symbols
989 represent measurements affected by cracks. The dotted line represents major zones in CL.
990 The corresponding CL images are shown in Fig. S1(data repository).

991 **Figure 9.** Cathodoluminescence images of zircons. The red ellipses indicate the location of the
992 $\delta^{18}O$ SIMS analyses (error 2σ).

993 **Figure 10.** Oxygen isotope values of single zircon phenocrysts measured by SIMS. The error
994 (2σ) is usually better than 0.3 ‰. The zircon population of a single sample shows a large
995 spread, but no differences exist between individual samples. Rim and core from one zircon
996 are usually the same within the error. Horizontal lines represent the sample average.

997 **Figure 11.** Calculated oxygen isotope fractionation for **(a)** quartz-whole rock, and **(b)** quartz-
998 zircon. Full symbols represent bulk quartz measured with CO_2-laser fluorination and open
999 symbols represent quartz measured with SIMS. Whole rock analysis was obtained by laser
1000 fluorination. Zircon crystals were all measured with SIMS. The 700°C and 900°C line is the
1001 calculated equilibrium fractionation based on the values as indicated in Tab. 3. The 2σ of the
1002 analyses is indicated, where not shown it is smaller than symbol.

1003 **Figure 12.** Histogram of $\delta^{18}O$-values from **(a)** quartz and **(b)** zircon. The average quartz has a
1004 value of 11.6 ‰ and the average zircon has a value of 8.7 ‰.

1005 **Figure 13.** Temperature versus time plot for oxygen isotope (Giletti and Yund 1984) and
1006 titanium (Cherniak et al. 2007) diffusion in quartz parallel to the c-axis over 500 μm. The
1007 diffusion time was calculated using the formula $t = 0.4*a^2/D$ for a sphere, a is the grain
1008 radius and D the diffusion coefficient. This corresponds to a 98 % exchange of the
1009 composition (Bloch and Ganguly, 2014)

1010 **Figure 14.** Comparison of the melt $\delta^{18}O$ value of the El Quemado Complex with other high $\delta^{18}O$
1011 silicic melts. Compilation after Folkes et al. 2013 and references therein. SCSG – Scottish
1012 Caledonian S-type granites (Appleby et al. 2010), Kamchatka (Bindeman et al. 2004), APVC
1013 – Altiplano Puna Volcanic Complex, GBT – Great Basin Tuff, TVZ – Topa Volcanic Zone,
1014 BT – Bishop Tuff, HRT – Huckleberry Ridge Tuff.

Always consult and cite the final, published document. See http:/www.minsocam.org or GeoscienceWorld

Table 1. Representative whole rock geochemical analyses of major elements (XRF).

Table 2a. Oxygen isotope analyses of the El Quemado Complex measured by laser fluorination (whole rock and quartz) and SIMS (quartz and zircon).

Table 2b. Summary of oxygen isotope profiles measured in quartz crystals from the El Quemado Complex by SIMS.

Table 3. Equilibrium oxygen isotope fractionation between quartz and rhyolite, quartz and zircon, and rhyolite and zircon at 900°C and 700°C.

Supplement Figure S1. Additional cathodoluminescence images of quartz phenocrysts from rhyolitic lava flows and ignimbrites. The red dots indicate the location of the $\delta^{18}O$ SIMS analysis. All corresponding profiles are shown in Figure 8.

Supplement Figure S2. Calculated oxygen isotope fractionation for zircon-whole rock. Whole rock analysis was obtained by laser fluorination. Zircon crystals were all measured with SIMS. The 700°C and 900°C line is the calculated equilibrium fractionation based on the values as indicated in Tab. 3. The 2σ of the analysis is indicated, where not shown it is smaller than symbol.

Supplement Table S1. SIMS $\delta^{18}O$ data of all profiles measured on quartz samples from rhyolitic lava flows and ignimbrites of the El Quemado Complex (profiles are shown in Figures 6 to 8).

Always consult and cite the final, published document. See http:/www.minsocam.org or GeoscienceWorld

This is a preprint, the final version is subject to change, of the American Mineralogist (MSA)
Cite as Authors (Year) Title. American Mineralogist, in press.
DOI: https://doi.org/10.2138/am-2018-6520

Figure 1

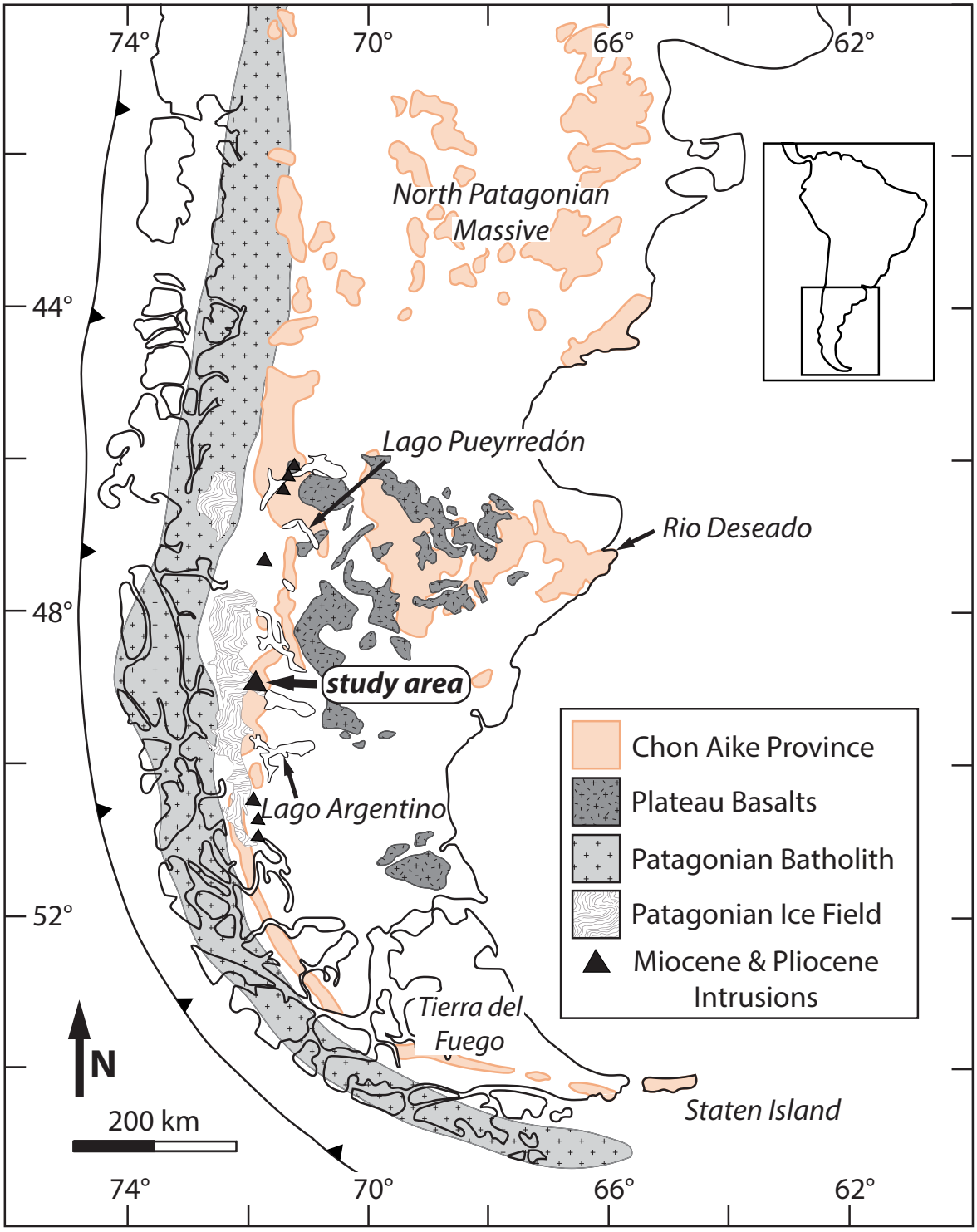

Always consult and cite the final, published document. See http:/www.minsocam.org or GeoscienceWorld

This is a preprint, the final version is subject to change, of the American Mineralogist (MSA)
Cite as Authors (Year) Title. American Mineralogist, in press.
DOI: https://doi.org/10.2138/am-2018-6520

Figure 2

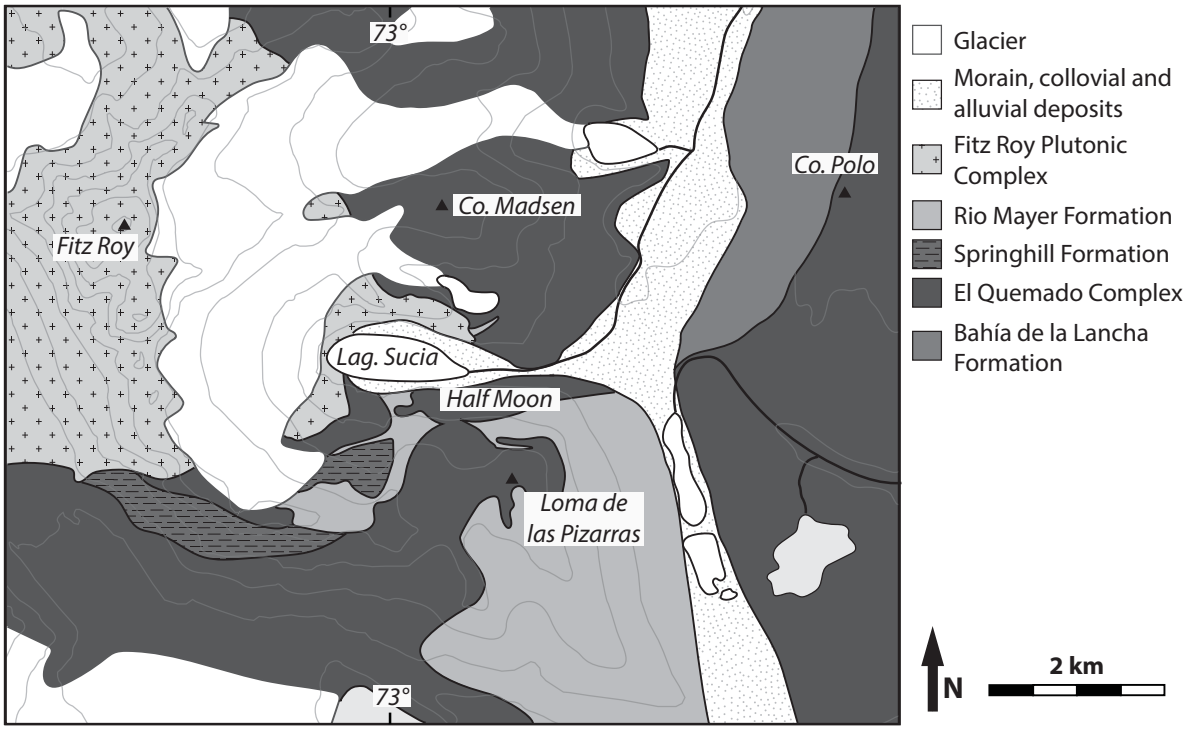

Always consult and cite the final, published document. See http:/www.minsocam.org or GeoscienceWorld

This is a preprint, the final version is subject to change, of the American Mineralogist (MSA)
Cite as Authors (Year) Title. American Mineralogist, in press.
DOI: https://doi.org/10.2138/am-2018-6520

Figure 3

Always consult and cite the final, published document. See http:/www.minsocam.org or GeoscienceWorld

This is a preprint, the final version is subject to change, of the American Mineralogist (MSA)
Cite as Authors (Year) Title. American Mineralogist, in press.
DOI: https://doi.org/10.2138/am-2018-6520

Figure 4

Always consult and cite the final, published document. See http:/www.minsocam.org or GeoscienceWorld

This is a preprint, the final version is subject to change, of the American Mineralogist (MSA)
Cite as Authors (Year) Title. American Mineralogist, in press.
DOI: https://doi.org/10.2138/am-2018-6520

Figure 5

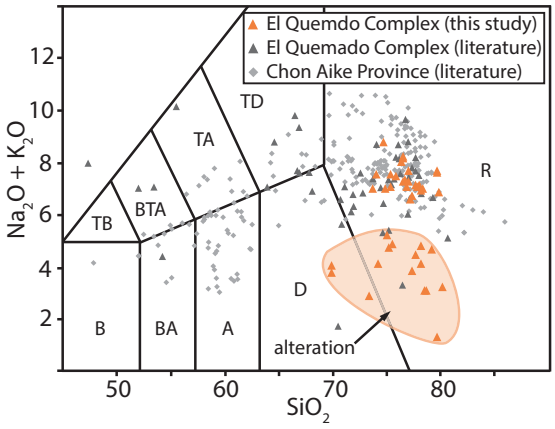

Always consult and cite the final, published document. See http:/www.minsocam.org or GeoscienceWorld

This is a preprint, the final version is subject to change, of the American Mineralogist (MSA)
Cite as Authors (Year) Title. American Mineralogist, in press.
DOI: https://doi.org/10.2138/am-2018-6520

Figure 6

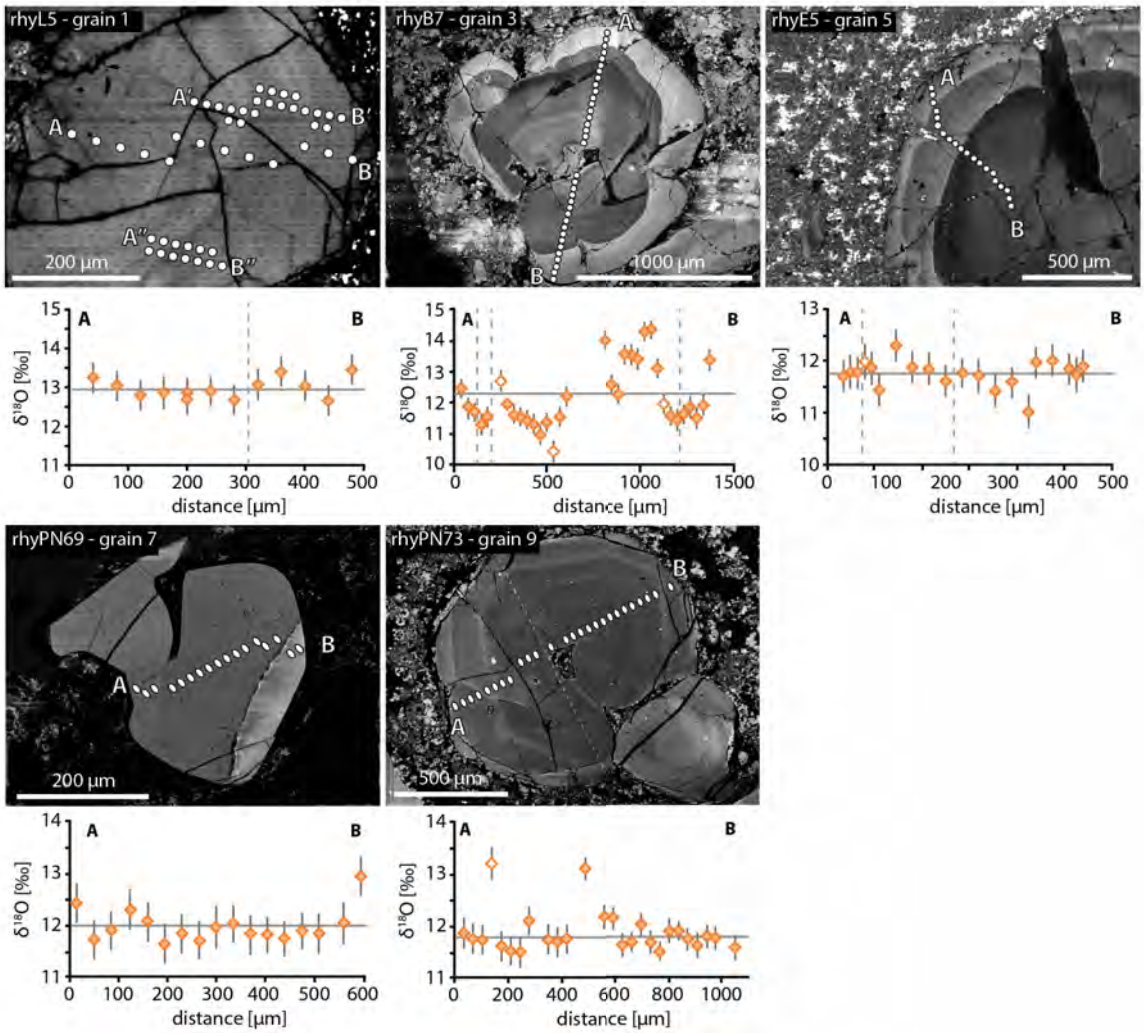

Always consult and cite the final, published document. See http:/www.minsocam.org or GeoscienceWorld

This is a preprint, the final version is subject to change, of the American Mineralogist (MSA)
Cite as Authors (Year) Title. American Mineralogist, in press.
DOI: https://doi.org/10.2138/am-2018-6520

Figure 7

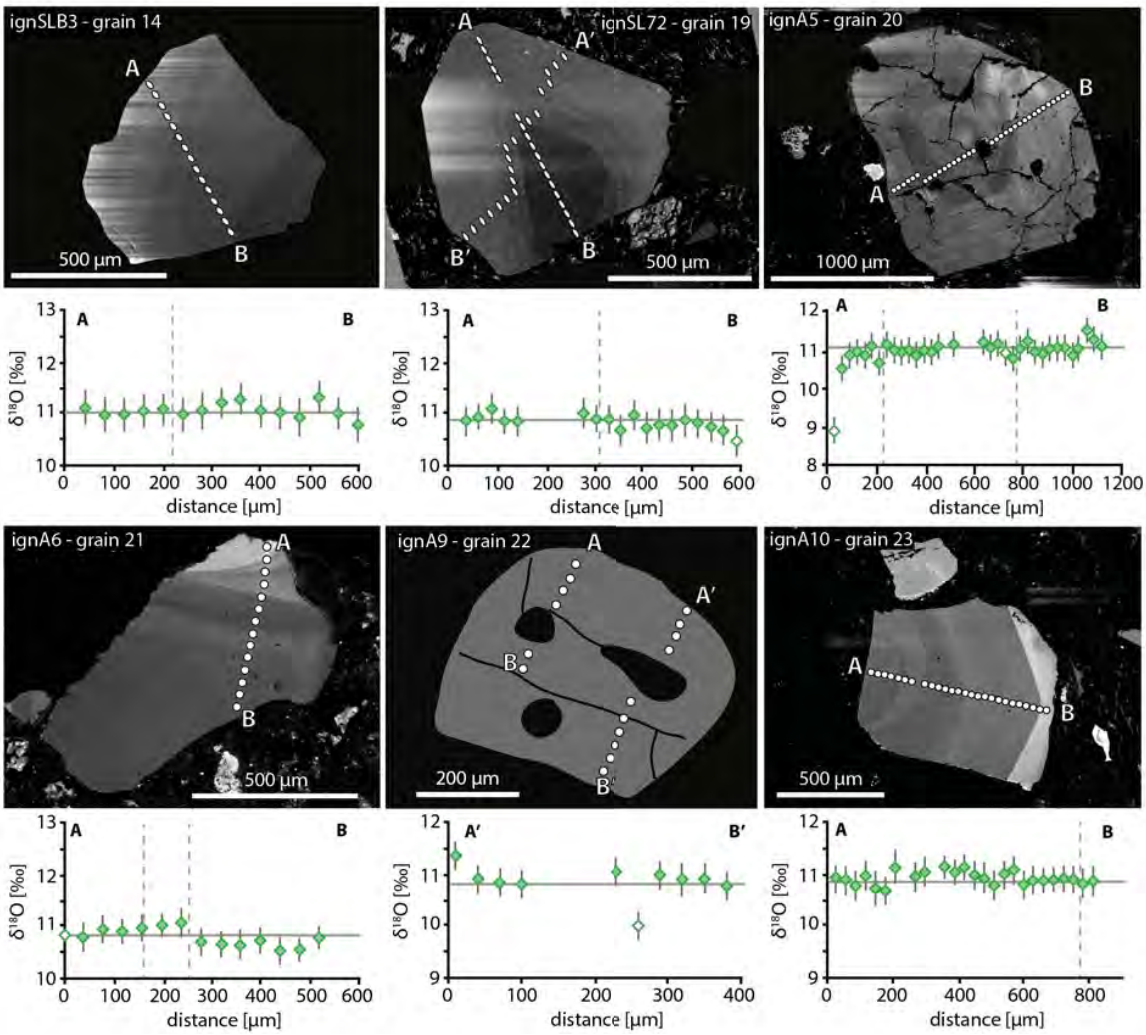

Always consult and cite the final, published document. See http:/www.minsocam.org or GeoscienceWorld

This is a preprint, the final version is subject to change, of the American Mineralogist (MSA)
Cite as Authors (Year) Title. American Mineralogist, in press.
DOI: https://doi.org/10.2138/am-2018-6520

Figure 8

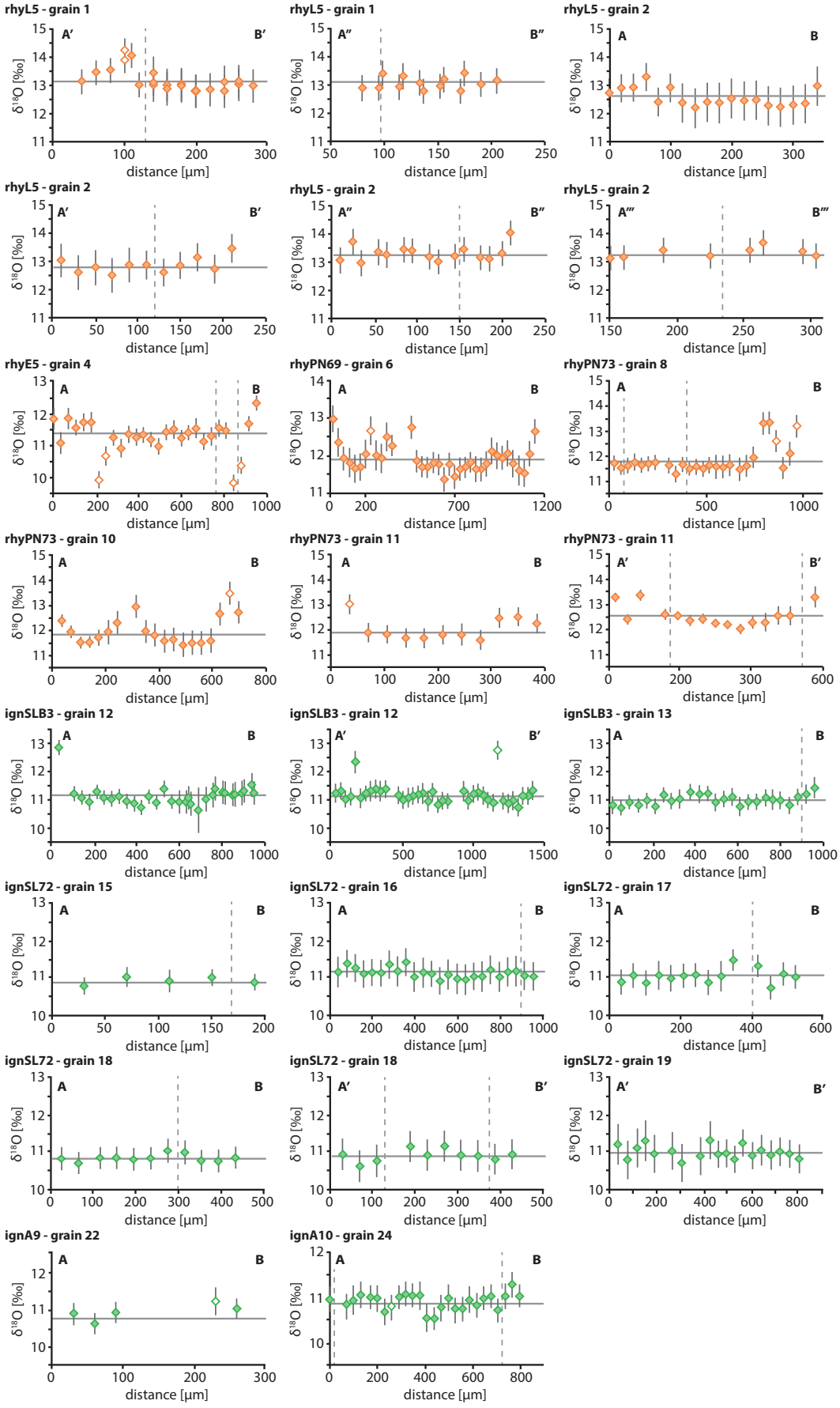

Always consult and cite the final, published document. See http:/www.minsocam.org or GeoscienceWorld

This is a preprint, the final version is subject to change, of the American Mineralogist (MSA)
Cite as Authors (Year) Title. American Mineralogist, in press.
DOI: https://doi.org/10.2138/am-2018-6520

Figure 9

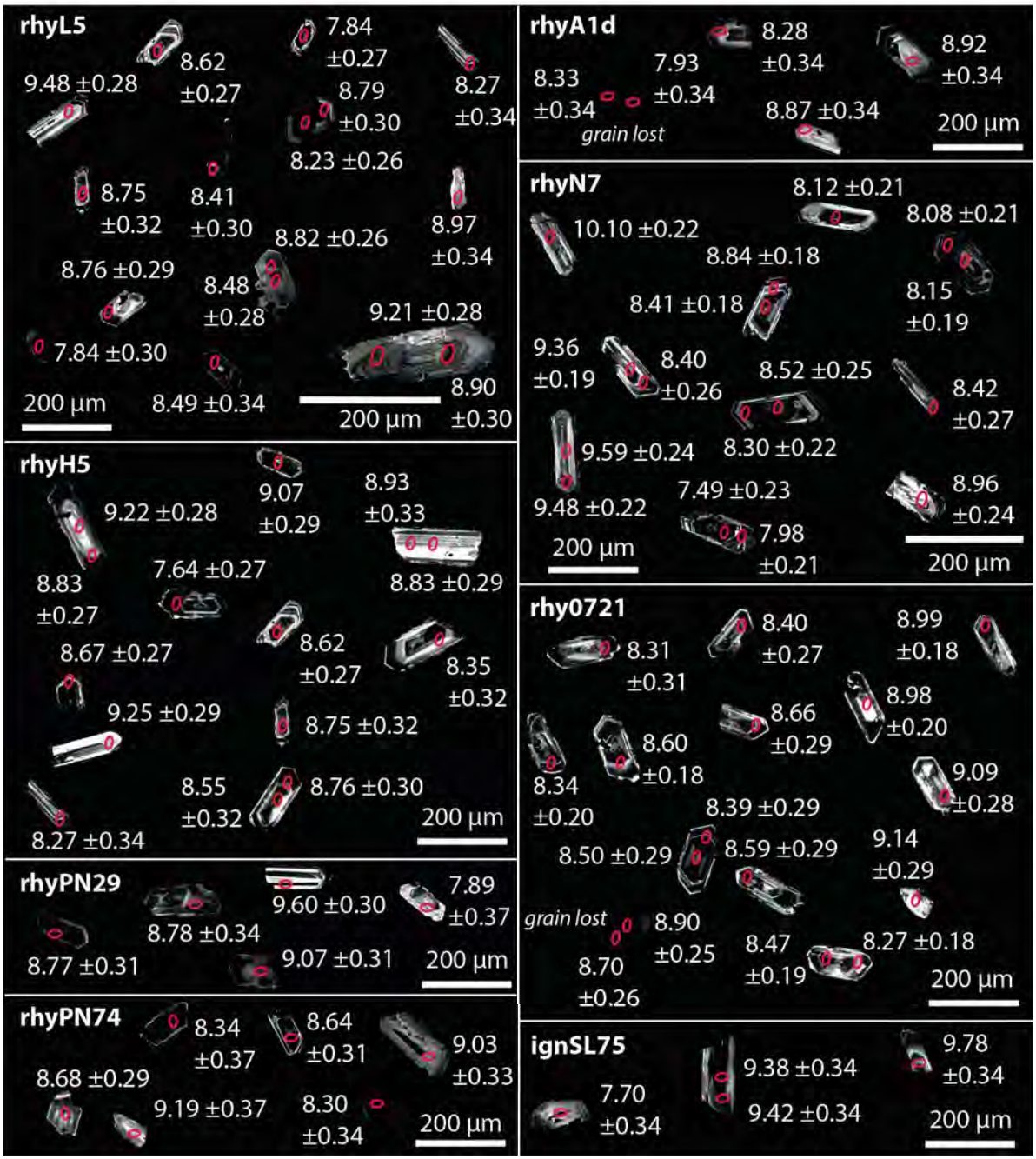

Always consult and cite the final, published document. See http:/www.minsocam.org or GeoscienceWorld

This is a preprint, the final version is subject to change, of the American Mineralogist (MSA)
Cite as Authors (Year) Title. American Mineralogist, in press.
DOI: https://doi.org/10.2138/am-2018-6520

Figure 10

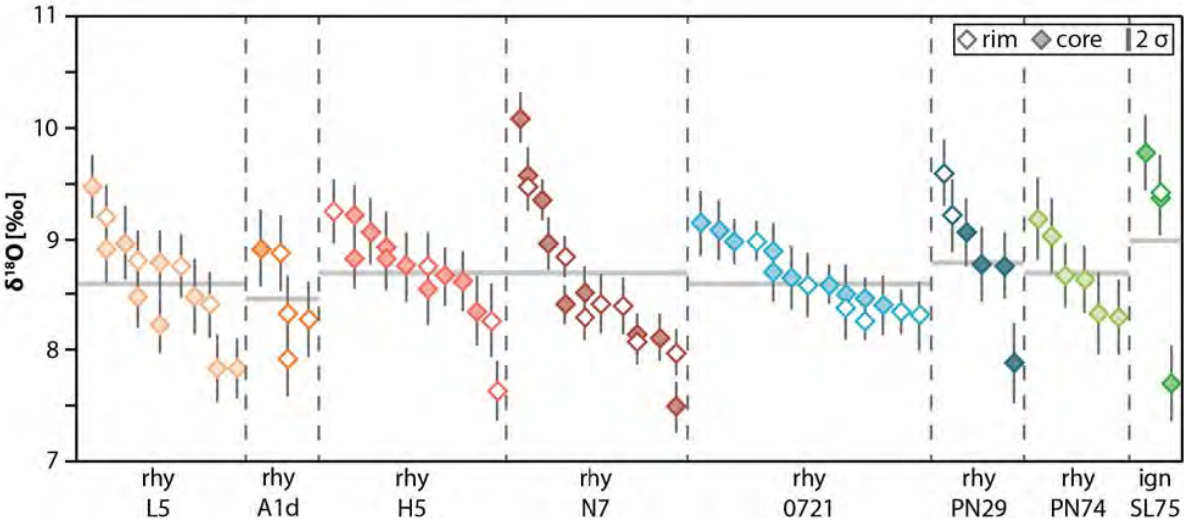

Always consult and cite the final, published document. See http:/www.minsocam.org or GeoscienceWorld

This is a preprint, the final version is subject to change, of the American Mineralogist (MSA)
Cite as Authors (Year) Title. American Mineralogist, in press.
DOI: https://doi.org/10.2138/am-2018-6520

Figure 11

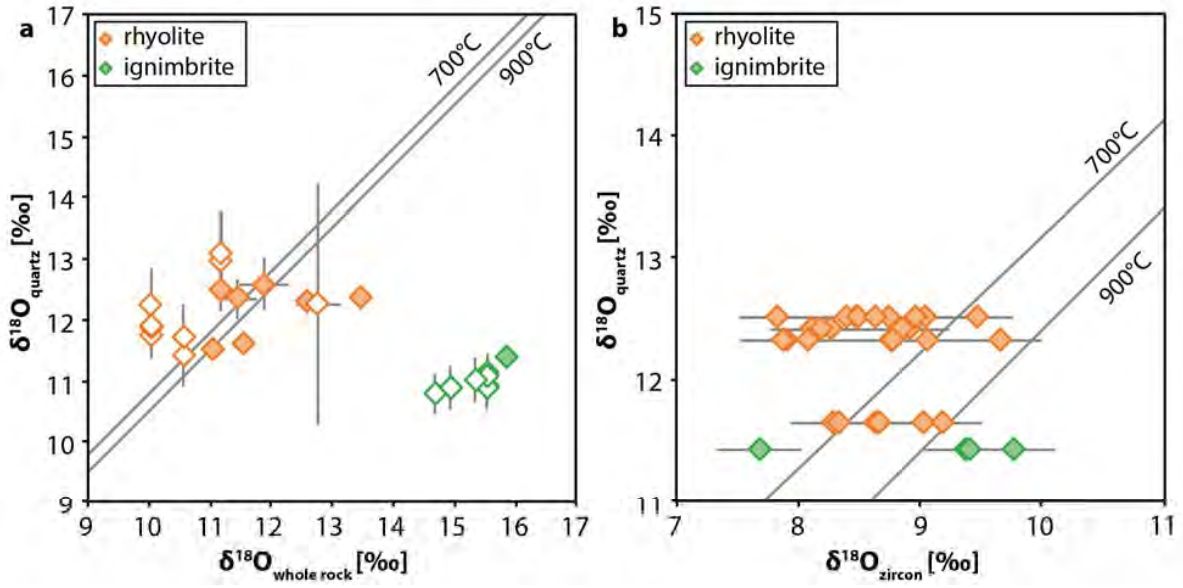

Always consult and cite the final, published document. See http:/www.minsocam.org or GeoscienceWorld

This is a preprint, the final version is subject to change, of the American Mineralogist (MSA)
Cite as Authors (Year) Title. American Mineralogist, in press.
DOI: https://doi.org/10.2138/am-2018-6520

Figure 12

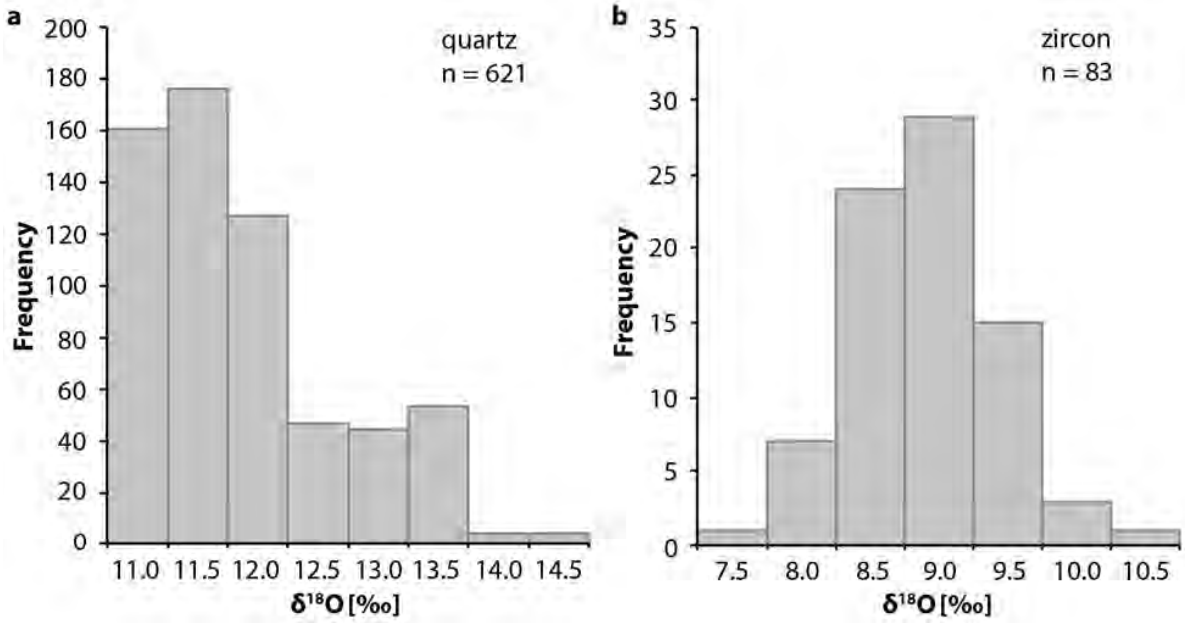

Always consult and cite the final, published document. See http:/www.minsocam.org or GeoscienceWorld

This is a preprint, the final version is subject to change, of the American Mineralogist (MSA)
Cite as Authors (Year) Title. American Mineralogist, in press.
DOI: https://doi.org/10.2138/am-2018-6520

Figure 13

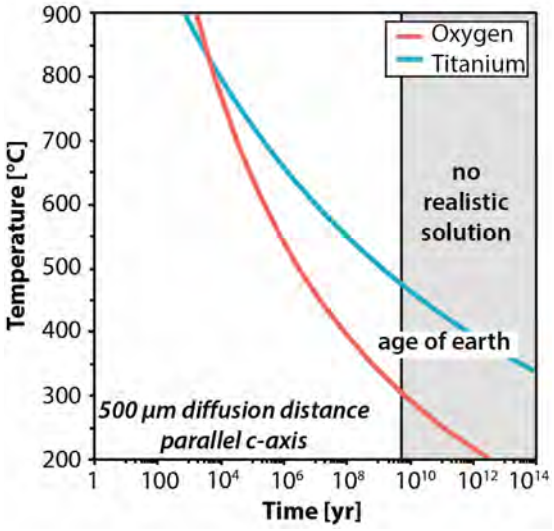

Always consult and cite the final, published document. See http:/www.minsocam.org or GeoscienceWorld

This is a preprint, the final version is subject to change, of the American Mineralogist (MSA)
Cite as Authors (Year) Title. American Mineralogist, in press.
DOI: https://doi.org/10.2138/am-2018-6520

Figure 14

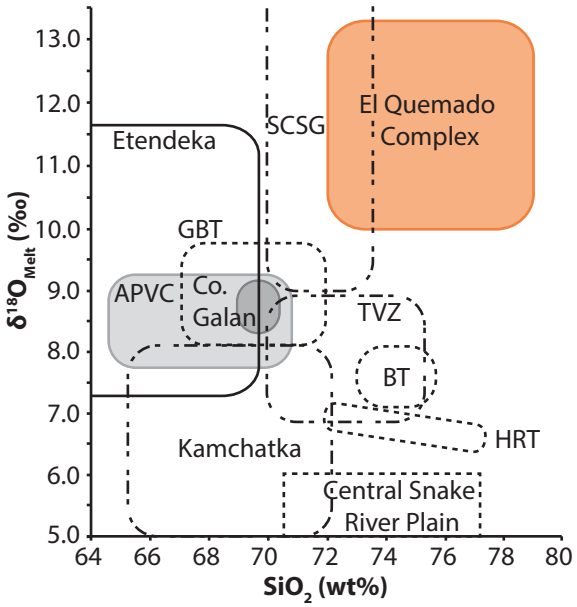

Always consult and cite the final, published document. See http:/www.minsocam.org or GeoscienceWorld

This is a preprint, the final version is subject to change, of the American Mineralogist (MSA)
Cite as Authors (Year) Title. American Mineralogist, in press.
DOI: https://doi.org/10.2138/am-2018-6520

Sample	rhyL5	rhyA1d	rhyN7	rhy0721	rhy0821	rhySL30	rhyPN74	rhyPN29	ignSL72	ignA5	ignSL75
Locality	Co. Madsen			Laguna Sucia		Half Moon	Lomo de las Pizarras		Co. Polo		
SiO2	77.21	79.24	75.80	77.45	78.39	76.49	76.07	75.22	75.08	73.22	77.73
TiO2	0.05	0.05	0.09	0.05	0.08	0.05	0.09	0.08	0.11	0.08	0.22
Al2O3	12.95	12.00	13.00	12.66	13.12	11.84	13.48	13.38	11.13	9.93	8.69
Fe2O3(t)	1.41	0.18	1.79	0.93	0.79	1.25	1.18	1.70	1.96	1.76	8.28
MnO	0.02	0.00	0.03	0.02	0.00	0.01	0.02	0.01	0.05	0.06	0.04
MgO	0.11	0.02	0.47	0.06	0.06	0.60	0.14	0.11	0.66	0.68	1.11
CaO	0.33	0.08	0.68	0.58	0.16	1.95	1.19	0.21	3.41	4.69	0.21
Na2O	2.19	2.62	2.36	2.76	0.78	2.11	2.59	2.38	0.36	0.73	0.32
K2O	4.92	5.05	4.77	4.37	6.39	2.45	4.65	5.50	2.67	2.22	1.06
P2O5	0.02	0.02	0.02	0.02	0.02	0.03	0.03	0.02	0.03	0.01	0.02
LOI	0.61	0.53	0.59	0.60	0.32	3.23	0.37	0.99	4.51	5.89	2.18
Total	99.82	99.78	99.59	99.51	100.10	100.00	99.81	99.60	99.97	99.28	99.86

Always consult and cite the final, published document. See http:/www.minsocam.org or GeoscienceWorld

This is a preprint, the final version is subject to change, of the American Mineralogist (MSA)
Cite as Authors (Year) Title. American Mineralogist, in press.
DOI: https://doi.org/10.2138/am-2018-6520

	δ¹⁸O (laser fluorination)				δ¹⁸O (SIMS)					
Sample	**WR [‰]**		**Qtz [‰]**		**Qtz [‰]**		**n**	**Zrc [‰]**		**n**
Cerro Madsen - Rhyolites										
rhyL5	11.18		12.49	± 0.01	13.01	± 0.74	95	8.63	± 0.97	13
rhyA1d	13.48		12.39					8.47	± 0.84	5
rhyL4	11.46		12.37	± 0.16						
rhyD1c			12.12	± 0.05						
rhyL6	12.07									
rhyC1	11.90									
Laguna Sucia - Rhyolites										
rhyH5	12.15	± 0.10						8.70	± 0.83	14
rhyN7	10.71	± 0.15						8.71	± 1.29	15
rhy0721*	11.95	± 0.38						8.64	± 0.58	17
rhySL38**	11.91		12.61	± 0.21						
rhy0821*	12.15	± 0.19								
rhySL62**	12.18									
rhyPN15**	10.64	± 0.14								
rhy0701*	13.14									
rhy0786*	13.48	± 0.32								
Half Moon - Rhyolites										
rhyB7	12.80	± 0.18			12.28	± 1.97	29			
rhyE5	10.60				11.58	± 0.66	43			
rhyPN29**	12.58		12.30	± 0.06				8.79	± 0.26	9
rhyN1a	11.04	± 0.10	11.54							
rhyPN31**	10.84									
Loma de las Pizarras - Rhyolites										
rhyPN69**					11.94	± 0.35	52			
rhyPN73**	10.04				11.95	± 0.99	89			
rhyPN74**	11.55		11.62					8.7	± 0.72	6
rhyPN26**	12.32	± 0.40	11.23							
rhyPN10**	12.61									
Corro Polo - Ignimbrites										
ignSLB3**					11.11	± 0.55	107			
ignSL72**	15.54		11.02		10.99	± 0.37	99			
ignA5	15.34	± 0.03			11.04	± 0.37	31			
ignA6	14.68				10.79	± 0.36	13			
ignA9	14.96				10.95	± 0.35	13			
ignA10	14.93				10.91	± 0.31	50			
ignSL75**	15.7	± 0.22	11.40					9.07	± 1.87	4
ignSL71**	15.64	± 0.31								

Errors for laser fluorination analysis are reported as 1σ.
If no duplicates were analyzed, laser fluorination data is reported with 0.1‰ (1σ) by default.
Errors for the SIMS analysis are reported as 2σ.
WR - whole rock; Qtz - quartz; Zrc - zircon
samples from: * Ramírez de Arellano 2011; **Leresche 2013 or Nescher 2013

Always consult and cite the final, published document. See http:/www.minsocam.org or GeoscienceWorld

This is a preprint, the final version is subject to change, of the American Mineralogist (MSA)
Cite as Authors (Year) Title. American Mineralogist, in press.
DOI: https://doi.org/10.2138/am-2018-6520

sample name	grain	transect	#	$\delta^{18}O$ [‰]	STDV 2σ	n	comments
Cerro Madsen - Rhyolites							
rhyL5				**13.01**	**± 0.74**	**95**	sample average
grain_01	1			13.07	± 0.55	45	grain average
		A-B	1	12.98	± 0.53	13	
		A'-B'	2	13.14	± 0.62	19	
		A''-B''	3	13.06	± 0.44	13	
grain_04	2			12.95	± 0.87	50	grain average
		A-B	4	12.57	± 0.62	18	
		A'-B'	5	12.85	± 0.55	11	
		A''-B''	6	13.32	± 0.57	14	
		A'''-B'''	7	13.35	± 0.36	7	
Half Moon - Rhyolites							
rhyB7	3		8	**12.28**	**± 1.97**	**29**	sample average
rhyE5				**11.58**	**± 0.66**	**43**	sample average
grain_01	4		9	11.44	± 0.63	24	
grain_07	5		10	11.75	± 0.53	19	
Loma de las Pizarras - Rhyolites							
rhyPN69* **				**11.94**	**± 0.35**	**52**	sample average
grain 69a	6		11	11.91	± 0.73	35	
grain 69b	7		12	12	± 0.64	17	
rhyPN73* **				**11.95**	**± 0.99**	**89**	sample average
grain 73	8		13	11.79	± 1.01	24	
grain 73a	9		14	11.82	± 0.66	25	
grain 73b	10		15	11.94	± 0.95	18	
grain 73c	11			12.29	± 1.06	22	grain average
		A-B	16	11.94	± 0.68	10	
		A'-B'	17	12.59	± 0.94	12	
Cerro Polo - Ignimbrites							
ignSLB3* **				**11.11**	**± 0.55**	**107**	sample average
grain a	12			11.16	± 0.63	67	grain average
		A-B	18	11.16	± 0.75	31	
		A'-B'	19	11.16	± 0.53	36	
grain b	13		20	11.00	± 0.36	25	
grain c	14		21	11.05	± 0.27	15	
ignSL72* **				**10.99**	**± 0.37**	**99**	sample average
grain a	15		22	10.92	± 0.20	5	
grain b	16		23	11.15	± 0.26	24	
grain c	17		24	11.08	± 0.38	14	
grain d	18			10.98	± 0.26	21	grain average
		A-B	25	10.86	± 0.19	11	
		A'-B'	26	10.92	± 0.32	10	
grain e	19			10.92	± 0.33	36	grain average
		A-B	27	10.84	± 0.23	17	
		A'-B'	28	10.98	± 0.35	19	
ignA5*	20		29	**11.04**	**± 0.37**	**31**	sample average
ignA6*	21		30	**10.79**	**± 0.36**	**13**	sample average
ignA9**	22			**10.95**	**± 0.35**	**13**	sample average
		A-B	31	10.88	± 0.35	4	
		A'-B'	32	10.98	± 0.35	9	
ignA10**				**10.91**	**± 0.31**	**50**	sample average
grain_05	23		33	10.90	± 0.25	25	
grain_10	24		34	10.92	± 0.36	25	

* from same ignimbrite layer 9
** from same ignimbrite layer 8

Always consult and cite the final, published document. See http:/www.minsocam.org or GeoscienceWorld

This is a preprint, the final version is subject to change, of the American Mineralogist (MSA)
Cite as Authors (Year) Title. American Mineralogist, in press.
DOI: https://doi.org/10.2138/am-2018-6520

	1000lnα		
Material	**900°C**	**700°C**	**Reference**
Qtz-rhy	0.6	0.9	3
	0.7	1.0	3+2
	0.5	***0.8***	***3+1****
	0.8	1.1	4+3
	-0.3	0.6	5+3
Qtz-Zrc	***2.4***	***3.3***	***4****
	1.9	2.8	6
	1.7	2.5	7
	1.1	1.5	8
	2.2	3.8	5+4
	1.5	1.8	5+8
rhy-Zrc	2.5	3.2	3+4

Qtz - quartz; Zrc - zircon; rhy - rhyolite
* values used for calculations in Fig. 11
(1) Appora et al. 2003; (2) Palin et al. 1996;
(3) Zhao and Zheng 2003; (4) Zheng 1996;
(5) Sharp and Kirschner 1994; (6) Valley 2003;
(7) Trail et al. 2009; (8) Krylov et al. 2002

Always consult and cite the final, published document. See http:/www.minsocam.org or GeoscienceWorld